REVIEW

Check for updates

From surface chemistry to ion dynamics: mechanistic roles of MXenes in aqueous zinc-ion batteries

Jinshuai Liu, Song Chen, Wenshuo Shang and Jintao Zhang [ID] *

As the global demand for sustainable and safe energy storage solutions intensifies, aqueous zinc-ion batteries (AZIBs) have emerged as a promising next-generation energy storage system owing to their inherent safety, cost-effectiveness, and environmental benignity. Metallic zinc, with a high theoretical capacity (820 mAh g^{-1}), a low redox potential, and natural abundance, is well-suited for use as an anode. However, persistent challenges, including dendrite growth, parasitic hydrogen evolution, and corrosion, undermine its long-term electrochemical stability. Meanwhile, cathode performance is often limited by structural degradation and sluggish Zn^{2+} diffusion kinetics. In this context, MXenes, a rapidly expanding family of two-dimensional (2D) transition metal carbides and nitrides, offer new opportunities for advancing AZIB technologies. Their unique structural characteristics, including high electrical conductivity, tunable interlayer spacing, and surface-rich functionalities, position them as promising candidates for both anode and cathode design. This review systematically elucidates the charge storage mechanisms in AZIBs, summarizes the development of advanced cathode and anode materials, and provides a critical overview of MXene synthesis, surface modification, and integration strategies. Particular emphasis is placed on their multifunctional roles in electrode frameworks and as electrolyte additives to modulate ionic conductivity and interfacial stability. By integrating recent insights and highlighting future research directions, this review aims to provide a roadmap for the rational design of MXene-enabled AZIBs with enhanced electrochemical reversibility, structural durability, and system-level performance.

Broader content

Aqueous zinc-ion batteries (AZIBs) offer intrinsic safety, low cost, and environmental compatibility. Yet, issues like dendrite growth, sluggish ion transport, and electrode degradation limit their performance. MXenes, 2D transition metal carbides/nitrides, present unique advantages such as high conductivity, tunable interlayer spacing, and functional surfaces for improving electrode and interfacial stability. This review outlines the fundamental charge storage mechanisms, highlights recent progress in AZIB design, focusing on MXene synthesis, modification, and multifunctional integration. It also explores their broader potential in multivalent systems, offering guidance for next-generation battery development.
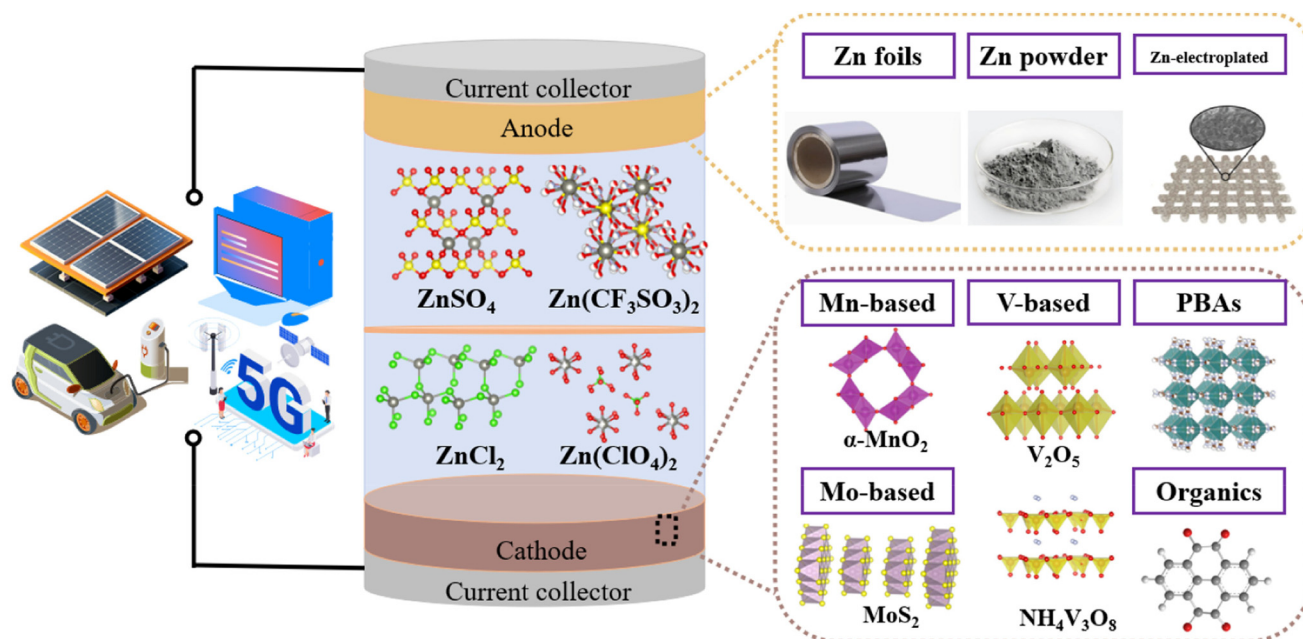
1. Introduction

With the rapid advancement of the global economy and continuous technological progress, the demand for energy has surged dramatically. However, the traditional fossil fuels such as coal, natural gas, and petroleum are finite and non-renewable resources. Their extensive consumption contributes substantially to greenhouse gas emissions, thereby intensifying

Key Laboratory for Colloid and Interface Chemistry Ministry of Education, School of Chemistry and Chemical Engineering, Shandong University, Jinan, 250100, P. R. China. E-mail: jtzhang@sdu.edu.cn

global warming and environmental pollution.[1,2] In response, clean and renewable energy sources such as solar, wind, and tidal energy have experienced significant growth. Nevertheless, their energy output is inherently intermittent and highly dependent on geographic and temporal conditions, which severely limit their stability and reliability in practical applications. To address this challenge, the development of efficient energy storage systems is essential to capture and store energy from diverse sources for continuous and controlled utilization. Among various energy storage technologies, lithium-ion batteries have emerged as the most widely used systems due to their high energy density and good cycling stability, and are widely deployed in electric vehicles, marine transport, and smart grids.[3] However, as the global energy

Fig. 1 The applications of typical AZIBs and the commercially used materials of the cathode, anode, and electrolyte. Reproduced with permission from ref. 10.

transition accelerates, the rising cost and limited availability of lithium resources have become increasingly critical concerns. These challenges underscore the urgent need to develop alternative energy storage technologies that are low-cost, resource-abundant, and inherently safe.

Aqueous-based batteries, utilizing water-based electrolytes, present several intrinsic advantages over traditional organic electrolyte systems. First, aqueous electrolytes allow for simple and safe battery assembly under ambient conditions, eliminating the need for inert or anhydrous environments and thereby substantially reducing production costs.[4] Second, the lower viscosity of aqueous electrolytes (~1 mPa s) compared to their organic counterparts (~1.9 mPa s) facilitates faster ion transport, leading to higher power density and fast charging capability.[5] Third, the non-toxic, non-volatile, and non-flammable nature of aqueous electrolytes significantly enhances operational safety. These merits have drawn increasing attention toward aqueous rechargeable batteries.[6] Aqueous battery systems can be broadly categorized based on the valence state of the charge carriers involved. Monovalent ion systems (e.g., Li^+, Na^+, and K^+) typically involve single electron transfer processes, while multivalent ion systems (e.g., Zn^{2+}, Mg^{2+}, Ca^{2+}, and Al^{3+}) enable multiple-electron transfers, thereby offering higher theoretical capacities. Despite their promise, many multivalent ion systems face fundamental challenges that hinder practical application. For instance, Mg^{2+} suffers from poor reversibility in deposition/stripping processes within aqueous electrolytes,[7] Ca^{2+} exhibits sluggish kinetics due to its large hydrated ionic radius (~1.00 Å),[8] and Al^{3+} is prone to form passivation layers that impede cycling stability.[9] In contrast, Zn^{2+} stands out due to its favorable combination of pro-

perties, including high theoretical capacity, low cost, and environmental compatibility. As such, zinc-ion batteries have garnered considerable attention as promising next-generation energy storage systems.

The typical configuration and material components of AZIBs are illustrated in Fig. 1.[10] Metallic zinc can be directly employed as the anode owing to its high theoretical specific capacity, suitable redox potential, and low cost.[11] However, several issues challenge the practical deployment of zinc anodes. The uneven electric field distribution on the zinc surface often leads to non-uniform Zn^{2+} deposition, resulting in uncontrolled dendrite growth that may penetrate the separator and cause short circuits. Additionally, parasitic side reactions such as the HER and surface corrosion at the electrode and electrolyte interface severely degrade anode stability and reduce cycle life.[12] On the cathode side, the development of materials with high electrochemical stability and rapid reaction kinetics remains an ongoing challenge.[13]

MXenes are emerging two-dimensional (2D) materials with abundant surface terminations, tunable interlayer spacing, and excellent electrical conductivity. Although graphene exhibits ultra-high conductivity due to its zero bandgap, its chemically inert surface relies heavily on complex functionalization to introduce active sites.[14] In contrast, g-C_3N_4, as a semiconductor, suffers from limited charge carrier mobility and inherent structural brittleness, which restrict its electrochemical applications.[15] Compared to these materials, MXenes offer distinct advantages. Their rich surface chemistry can be directly tailored during the etching process, avoiding the need for the complicated post-treatment required for graphene. The dynamically adjustable interlayer spacing of MXenes over-

comes the diffusion limitations of large ions imposed by graphene's fixed interlayer distance. Furthermore, MXenes combine a Young's modulus comparable to graphene with superior flexibility, reinforcing their irreplaceable role in flexible devices.[16]

This review aims to provide a comprehensive overview of AZIBs from a fundamental perspective. We first introduce the historical development and underlying energy storage mechanisms of AZIBs, followed by a discussion of current challenges. Subsequently, we explore various cathode and anode material systems under investigation. Particular emphasis is placed on MXene-based materials, including their structural characteristics, synthetic strategies, and recent advances in AZIB applications. Finally, we summarize key developments and offer perspectives on the future outlook for MXene-enabled AZIB technologies.

2. Overview of aqueous zinc-ion batteries

2.1 Development history

As illustrated in Fig. 2, the evolution of AZIBs spans more than two centuries.[17,18] The earliest battery dates back to 1799, when Alessandro Volta invented the first voltaic pile by stacking alternating zinc and copper discs separated by brine-soaked cloth.[3] In 1836, John Frederic Daniell developed the first practical Zn–Cu battery, which found practical application in railway signaling and marked a significant advancement in battery technology.[19] In 1866, Georges Leclanché introduced a new Zn–MnO$_2$ battery, utilizing a zinc rod as the anode, MnO$_2$ as the cathode, and a 20% NH$_4$Cl aqueous solution as the electrolyte.[20] In 1885, Carl Gassner further improved this system

by adding starch to the electrolyte to form a paste, solving leakage issues and ushering in the era of dry cells.[15] In 1986, Yamamoto pioneered the replacement of corrosive KOH with neutral ZnSO$_4$, leading to an aqueous Zn–Mn battery capable of nearly 50 charge–discharge cycles.[21] However, a complete understanding of the electrochemical mechanisms remained elusive until 2011, when Kang and colleague explored rechargeable AZIBs and elucidated their reaction pathways.[22] This significant discovery not only overcame the limitations of traditional zinc-ion batteries as primary cells but also propelled the rapid development of AZIB technology, establishing it as a vital branch in emerging energy storage systems.[23]

2.2 Energy storage mechanisms

AZIBs typically consist of a zinc metal anode, a suitable cathode material, a separator, and an aqueous electrolyte. During discharge, the metallic zinc anode oxidizes to Zn^{2+}, releasing electrons that flow through the external circuit, while Zn^{2+} ions diffuse towards the cathode through the electrolyte. The charging process reverses these reactions. The cathode reactions differ markedly from those in lithium-ion batteries and can be classified into three main mechanisms: Zn^{2+} insertion, Zn^{2+} and H$^+$ co-insertion, and conversion reactions.[24]

2.2.1 Zn^{2+} insertion mechanism. Cathode materials with open-framework or layered crystal structures can reversibly host Zn^{2+}. Upon discharge, Zn^{2+} ions are inserted into the cathode lattice alongside electrons to maintain charge balance. During charging, Zn^{2+} ions are extracted back into the electrolyte. The ionic radius of Zn^{2+} (0.74 Å) is similar to that of Li$^+$ (0.76 Å), allowing for reasonably efficient diffusion in suitable hosts.[25] For instance, a rechargeable Zn–MnO$_2$ battery was fabricated by using tunnel-structured α-MnO$_2$ as the

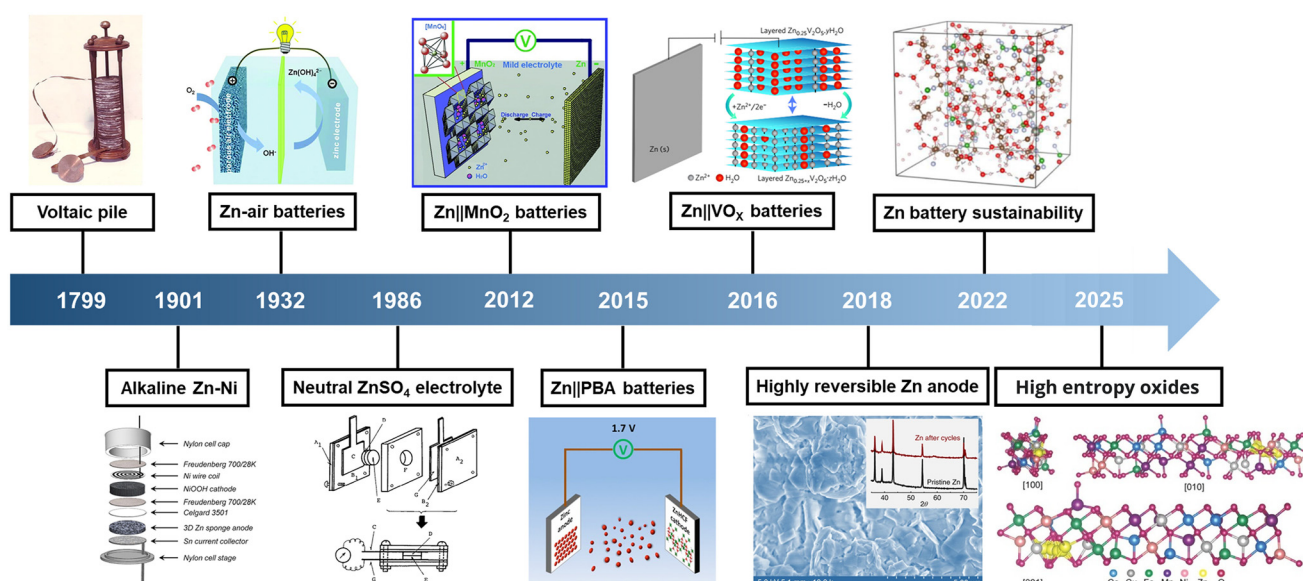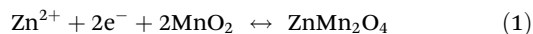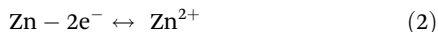**Fig. 2** A timeline demonstrating the development of AZIBs. Reproduced with permission from ref. 17 and 18.

cathode.[22] Zn^{2+} inserts into α-MnO_2 during discharge, forming $ZnMn_2O_4$, which reverts upon charging:

Cathode:

$$Zn^{2+} + 2e^- + 2MnO_2 \leftrightarrow ZnMn_2O_4 \qquad (1)$$

Anode:

$$Zn - 2e^- \leftrightarrow Zn^{2+} \qquad (2)$$

However, in aqueous solutions, Zn^{2+} typically forms hydrated complexes with a larger effective radius ($\sim$4.3 Å), resulting in slow kinetics due to strong electrostatic interactions. Using water-rich layered MnO_x, the interlayer water would weaken electrostatic interactions, facilitating Zn^{2+} diffusion and enhancing structural integrity.[26] Other examples include γ-MnO_2,[27] V_2O_5, p-VO_x@C, and Prussian blue analogs, all of which support Zn^{2+} insertion and demonstrate varying degrees of reversibility and capacity.[28]

2.2.2 Zn^{2+} and H^+ co-insertion mechanism. In some systems, both Zn^{2+} and H^+ participate in charge storage, offering synergistic effects. Due to their small size and high mobility, H^+ rapidly diffuses and inserts into the host material, while Zn^{2+} provides higher charge density. For example, a MoS_2/PEDOT composite with significantly expanded interlayer spacing was developed. The presence of PEDOT promoted H^+ insertion, which in turn weakened Zn^{2+} interactions with the host, improving ion transport.[29] Similarly, both Zn^{2+} and H^+ contributed to energy storage in a PEO-intercalated LiV_3O_8 cathode.[30] The PEO intercalation significantly increased the proportion and quantity of Zn^{2+} insertion, as evidenced by enhanced diffusion coefficients from GITT measurements.

Unlike the co-insertion of Zn^{2+} and H^+, Nazar reported a unique Zn^{2+}/H_2O co-intercalation mechanism in Zn–$Zn_{0.25}V_2O_5 \cdot nH_2O$ batteries.[31] The cathode material features a layered structure containing intercalated divalent metal ions and water molecules, along with dual-electron redox centers. Typically, water molecules are released simultaneously with Zn^{2+} insertion during discharge and are reabsorbed during charging. The reversible expansion and contraction of the interlayer spacing, enabled by H_2O molecules, plays a crucial role in facilitating reversible intercalation and deintercalation of Zn^{2+}. This dynamic contributes to enhanced reaction kinetics and excellent high-rate performance.

2.2.3 Conversion reaction mechanism. In contrast to the intercalation-based mechanisms described above, conversion reactions involve substantial structural phase transformations. These transformations allow the participation of multiple electrons in redox processes, enabling higher theoretical capacities. However, such conversions are often partially or wholly irreversible, which can result in rapid capacity degradation, thereby limiting the cycling stability and rate performance of conversion-type electrodes. Addressing this limitation requires thoughtful material design to enhance reversibility. For example, α-MnO_2 exhibited a morphological transition from micron-scale nanofibers to short nanorods and nanoparticle aggregates during the initial discharge.[32] This trans-

formation, differing from the previously reported formation of $ZnMn_2O_4$, was instead attributed to the reaction between α-MnO_2 and protons from the electrolyte, producing MnOOH according to the following reaction:

Cathode:

$$MnO_2 + H^+ + e^- \leftrightarrow MnOOH \qquad (3)$$

Anode:

$$Zn - 2e^- \leftrightarrow Zn^{2+} \qquad (4)$$

To maintain charge neutrality, the excess OH^- produced reacts with $ZnSO_4$ and H_2O in the electrolyte, forming flake-like $ZnSO_4[Zn(OH)_2]_3 \cdot xH_2O$. Similarly, β-MnO_2 is converted to MnOOH during the initial discharge.[33] The Mn^{2+} ions originate from both the dissolution of β-MnO_2 and the transformation of MnOOH. Upon charging, Mn^{2+} and MnOOH are reoxidized to ε-MnO_2, which can reversibly transition back to MnOOH or dissolve as Mn^{2+} under the influence of protons. Interestingly, both conversion reactions and Zn^{2+}/H^+ co-insertion processes coexist in α-MnO_2@CFP cathodes, revealing the presence of $ZnMn_2O_4$ and MnOOH phases during charge/discharge cycles.[34] Both studies highlight that the electrochemical behavior of MnO_2 in AZIBs involves far more than simple Zn^{2+} intercalation. Instead, it is a complex, multi-ion process involving H^+, Mn^{2+}, and structural transformations. Together, these studies offer complementary insights into MnO_2-based cathode chemistry, forming a robust theoretical foundation for future material design and system optimization. Going forward, efforts should focus on mitigating structural irreversibility and by-product formation, promoting efficient H^+/Zn^{2+} co-intercalation through morphological engineering, and formulating advanced electrolytes to stabilize electrode–electrolyte interfaces.

Each mechanism offers distinct benefits in terms of capacity, cycling stability, and rate capability, but also presents unique challenges. Moreover, these mechanisms may coexist or evolve dynamically during cycling, resulting in complex electrochemical behavior. Therefore, comprehensive mechanistic studies are essential to fully understand and optimize these storage processes, paving the way for the development of next-generation AZIBs. Several critical challenges continue to impede their practical implementation and commercialization. One of the primary issues lies in the instability of cathode materials, which often undergo dissolution, structural collapse, and volumetric expansion during repeated cycling. These degradation processes severely undermine the long-term cycling stability and contribute to rapid capacity fading. Furthermore, most cathode materials suffer from inherently low electronic conductivity. This limitation, combined with the strong electrostatic interaction between Zn^{2+} ions and the host framework, results in sluggish ion diffusion and poor rate performance. Compounding this issue, the ionic transport properties of separators and electrolytes are often insufficient, further hindering redox kinetics and overall cell efficiency.[35] On the anode side, the uncontrolled formation of zinc den-

drites remains a significant obstacle. Due to the tip effect, Zn^{2+} tends to deposit unevenly on surface protrusions, leading to dendrite growth that can eventually penetrate the separator and cause internal short circuits. Additionally, mechanical stress from repeated cycling can generate electrically isolated "dead zinc", diminishing both the reversibility and coulombic efficiency of the battery.[36] Another major concern is the proximity of the zinc deposition potential to that of the HER. This overlap makes it difficult to completely suppress the HER, even under an applied overpotential. The resulting gas evolution not only causes battery swelling and safety hazards but also increases the local pH, promoting the formation of corrosive byproducts that accelerate electrode degradation and reduce cycling life.[37]

3. Progress and overview of cathode materials

As a critical component of AZIBs, the cathode plays a central role in storing Zn^{2+} and largely determines the overall performance of the battery. To enable commercial deployment, cathode materials must exhibit excellent structural stability and long-term cycling durability. In recent years, considerable progress has been made in the development of high-performance cathode materials. A wide range of promising systems has emerged, including vanadium-based compounds, manganese-based compounds, Prussian blue analogs, organic materials and others.[38]

3.1 Vanadium-based compounds

Vanadium-based materials are considered promising cathodes for AZIBs due to their multiple valence states and diverse coordination environments, which provide exceptional flexibility in accommodating multivalent ions.[39] These materials can be broadly classified into vanadium oxides, metal vanadates, and other derivatives such as VS_2 and VSe_2.[40] Among them, V_2O_5, which utilizes a dual-electron V^{5+}/V^{3+} redox couple, offers a high theoretical capacity of 589 mAh g^{-1}, making it a compelling candidate for Zn^{2+} intercalation. However, the practical use of V_2O_5 is hindered by its inherently unstable layered structure and poor intrinsic electrical conductivity, which limit both its capacity retention and cycling stability. To overcome these limitations, several strategies have been proposed. For example, as illustrated in Fig. 3a, the addition of trimethyl phosphate (TMP) as an electrolyte additive reduces the free water content to just 2.5%, effectively suppressing parasitic reactions and vanadium dissolution, resulting in higher coulombic efficiency.[41] Particle size optimization is another effective approach. The ball-milled V_2O_5 used as a cathode in the $ZnSO_4$ electrolyte exhibited a high capacity of 410.2 mAh g^{-1} at 0.1 A g^{-1} along with excellent cycling performance.[42] Given the layered nature of V_2O_5, a polyaniline intercalation structure was developed to improve battery performance.[43] The intercalated conjugated polymer chains improve structural flexibility in confined interlayer spaces and
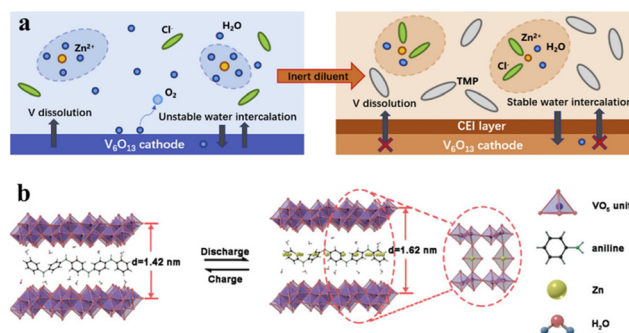
Fig. 3 (a) Schematic illustration of vanadium dissolution and CEI formation in a UWA electrolyte on a V_6O_{13} cathode during the electrochemical reactions. Reproduced with permission from ref. 41. (b) Schematic illustrations of zinc ion insertion/extraction of PANI100-V_2O_5 during the discharging/charging process. Reproduced with permission from ref. 43.

facilitate Zn^{2+} accommodation without significant phase transitions, thereby mitigating intercalation-induced stress and enhancing cycling durability (Fig. 3b).[43]

Compared to monovalent alkali metal ions, chemically pre-intercalated divalent metal ions form stronger ionic bonds with oxygen atoms, which helps bridge adjacent layers to prevent structural collapse. The $Zn_{0.25}V_2O_5 \cdot nH_2O$ cathode material was first demonstrated in AZIBs, delivering a reversible capacity of 260 mAh g^{-1} with 81% capacity retention over 1000 cycles. This breakthrough established hydrated vanadium oxides as promising cathode candidates for zinc-ion storage systems.[31] The co-intercalated water molecules buffer the high charge density of multivalent ions and reduce the activation energy for interfacial charge transfer. These water molecules play a crucial role in expanding and contracting the interlayer spacing reversibly, allowing efficient Zn^{2+} intercalation and deintercalation. Similarly, in $Mg_{0.34}V_2O_5 \cdot 0.84H_2O$, hydrated Mg^{2+} pillars enable the formation of an expanded interlayer spacing up to 13.4 Å, thereby facilitating rapid Zn^{2+} diffusion.[44] This exemplary "pillar effect" has inspired broad efforts to develop pre-intercalated hydrated vanadium oxides with enhanced electrochemical properties.[35]

Beyond oxides, other vanadium-based materials, such as layered sulfides and selenides, have also been employed as cathodes for AZIBs.[45,46] These compounds can accommodate Zn^{2+} *via* multiple redox processes, offering high energy density and rate performance. Despite their high theoretical capacity and cycling durability, the application of vanadium-based compounds in AZIBs still faces challenges, including low electrical conductivity and structural instability. Continued research efforts are therefore essential to fully exploit their potential in aqueous battery systems.

MXenes, with their exceptional intrinsic electrical conductivity, tunable surface functional groups (*e.g.*, –OH and –O), and excellent hydrophilicity, offer a promising opportunity to address the conductivity bottleneck and structural water management challenges of VO_x. When employed as conductive

scaffolds or coating layers, MXenes can significantly enhance the electron transport in VO$_x$ electrodes, thereby alleviating rate-performance limitations.[47] Moreover, the abundant oxygen-containing functional groups on MXenes can form strong interactions, such as hydrogen bonding, to effectively "anchor" structural water molecules, suppressing their detrimental dissociation and uncontrolled loss, and thus maintaining the stability of the hydrated structure. At the same time, the superior mechanical strength and layered architecture of MXenes help to distribute the stress induced by ion insertion more evenly, reinforcing the structural integrity of the VO framework. These synergistic effects ultimately contribute to improved cycling durability of VO-based cathodes, even under high-capacity operation.[48]

3.2 Manganese-based compounds

The advantages of manganese-based compounds primarily lie in their intrinsic safety, notable economic benefits, environmental friendliness, and abundant redox-active sites.[49] This material system encompasses various crystal structures, including multiple polymorphs of MnO$_2$ (α-, β-, γ-, ε-, δ-types) and manganese oxides such as Mn$_2$O$_3$, Mn$_3$O$_4$, and MnO.[50] These transition metal oxides exhibit highly reversible Zn^{2+} insertion and extraction behaviour during electrochemical cycling, attributed to their characteristic multi-electron transfer mechanisms, making them attractive candidates for emerging energy storage devices. However, their practical application is hindered by poor electrical conductivity and strong electrostatic interactions between Zn^{2+} and the host lattice, which result in sluggish ion migration. Moreover, due to the Jahn–Teller effect, Mn^{3+} ions tend to disproportionate into Mn^{2+} and Mn^{4+}, leading to Mn dissolution into the electrolyte and consequent voltage and capacity fading. Structurally, manganese-based compounds consist of single MnO$_x$ layers held together by weak van der Waals forces, which are prone to severe deformation, crystal structure damage, and irreversible phase transitions during repeated Zn^{2+} intercalation and deintercalation, further causing significant cycling instability.

Recent modification strategies have made notable progress in addressing these limitations. At the material design level, introducing specific ionic dopants (e.g., Mo, Al, and Ca^{2+}) has been shown to effectively mitigate these issues.[51] Mo and Al doping stabilizes higher manganese oxidation states (by increasing the average Mn valence), suppress Mn^{3+} disproportionation and Jahn–Teller distortions, and thus significantly enhance phase stability (Fig. 4).[52] Furthermore, Mo can widen interlayer spacing to facilitate Zn^{2+} diffusion, while Al induces special superlattice structures that improve both conductivity and ion diffusion kinetics, enabling exceptionally long cycling life (e.g., 15 000 cycles with 1.98% Al doping).[53] Ca^{2+} interlayer pillars stabilize the layered structure through a pillar effect, create oxygen vacancies, and improve reaction kinetics while maintaining structural integrity. Constructing 3D porous nanostructures (Ca$_{0.10}$MnO$_2$·0.61H$_2$O) offers a physical pathway to optimize Zn^{2+} transport and mitigate agglomeration-induced structural degradation.[54] Electrolyte engineering, such as NH$_4^+$
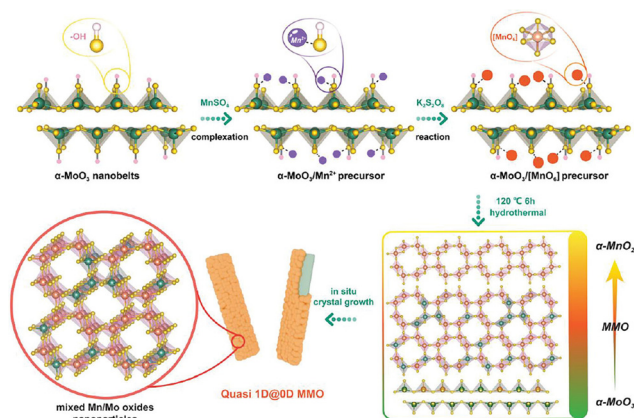

Fig. 4 Synthesis process of quasi 1D@0D mixed Mn/Mo oxides. Reproduced with permission from ref. 52.

pre-intercalation in tailored aqueous–organic hybrid electrolytes, also helps regulate interfacial reactions and charge-storage kinetics to limit manganese dissolution and related degradation.[55]

Importantly, as an emerging class of materials, 2D transition metal carbides/nitrides (MXenes) offer a promising route to address these challenges. Owing to their excellent electrical conductivity, tunable surface chemistry, abundant functional groups, and high hydrophilicity, MXenes can facilitate fast electron transfer and alleviate structural stress caused by charge accumulation. Their strong adsorption capability can help immobilize manganese ions or intermediates, effectively suppressing manganese dissolution.[39,56] Moreover, the layered structure of MXenes can act as a stable substrate or coating layer, guiding the controlled deposition/growth of MnO$_2$, mitigating adverse structural evolution, and enhancing phase stability. These unique properties present an attractive pathway to synergistically optimize ion diffusion, electronic conduction, and chemical or electrochemical stability – especially by suppressing manganese dissolution – in MnO$_2$-based zinc-ion batteries.

3.3 Prussian blue analogs

Prussian blue analogs (PBAs) are metal–organic frameworks characterized by the presence of internal metal centers and an ordered interconnected structure. Compared to layered metal oxides and polyanionic compounds, their lattices possess larger interstitial spaces that can accommodate metal ions with relatively larger ionic radii. The inherent 3D network structure effectively mitigates structural changes caused by repeated insertion and extraction of metal ions, endowing PBAs with high operating voltages and rapid charge and discharge capabilities. Early studies primarily explored Zn^{2+} storage hosts by tuning the metal centers, including orthorhombic ZnHCF,[57] cubic CuHCF,[58] FeHCF,[59] and NiHCF.[60] In 2015, it was reported that CuFe(CN)$_6$ could serve as a cathode for AZIBs, retaining 90% of its theoretical capacity after 100 cycles.[61] However, these metal hexacyanoferrates (MHCFs) gen-

erally exhibit low discharge capacities below 70 mAh g^{-1}. The limited Zn^{2+} storage sites within the tunnel-type structure, the solubility of active materials, and possible phase transitions and aging collectively result in poor cycling stability.

Recent strategies to improve the performance of PBAs highlight several effective approaches. In terms of morphology engineering, a self-templated method was innovatively employed to synthesize hollow Co-substituted manganese-based cobalt hexacyanoferrate (CoHCF) spheres (Fig. 5a), which demonstrate significant advantages.[62] The unique hollow architecture offers a large electrochemically active surface area and abundant ion (e.g., Zn^{2+}/K$^+$) transport channels. More importantly, the internal cavity effectively buffers the volumetric stress induced by repeated ion insertion/extraction, greatly enhancing the mechanical and structural stability. This design enables excellent rate capability and cycling durability, delivering a capacity of 173.4 mAh g^{-1} at 0.3 A g^{-1} with negligible decay even after 2200 cycles.[63] Lattice and compositional regulation represents another key strategy. In CoHCF, partial substitution of Mn^{3+} by Co^{2+} is crucial. Not only does Co^{2+} participate in redox reactions (Co^{2+}/Co^{3+}), but more importantly, it effectively suppresses Jahn–Teller distortions of the Mn–N$_6$ octahedra (arising from the d^4 high-spin configuration of Mn^{3+}), thereby significantly improving the cyclic phase stability of the framework. Defect engineering also shows strong potential. For example, precise control of the K$^+$/Ag$^+$ ratio in the framework enables the synthesis of vacancy-rich, anhydrous K$_{0.95}$Ag$_{3.05}$Fe(CN)$_6$ (Fig. 5b).[64] These anion vacancies not only optimize ion diffusion pathways but also activate two consecutive redox couples (Fe^{3+}/Fe^{2+} and Ag$^+$/Ag), theoretically involving up to 4 electrons per formula unit (2 from Fe(CN)$_6$ and 2 from Ag), resulting in an ultra-high theoretical capacity and 80.3% capacity retention after 100 cycles.

MXenes offer a promising pathway to address the remaining challenges of PBAs, such as limited conductivity, interfacial instability, and stress concentration during deep charge/discharge. MXenes, with their high electrical conductivity, tunable surface chemistry (e.g., abundant functional groups), and excellent mechanical properties, can serve as conductive scaffolds or coatings to enhance electron transport between PBA nanoparticles and distribute stress more uniformly.[60] Their strong surface interactions may help anchor the PBA framework, mitigating performance degradation due to component dissolution or vacancy migration. Additionally, the selective adsorption and transport of Zn^{2+} by MXenes may further improve interfacial kinetics. These synergistic effects make MXenes a highly promising platform for developing high-performance, long-life PBA-based cathodes for aqueous zinc-ion batteries.

### 3.4 Organic materials and others

Organic compounds, featuring high theoretical capacities, low cost, and low toxicity, have emerged as promising electrode materials for AZIBs. However, due to the weakly acidic nature of aqueous electrolytes and the repeated intercalation and deintercalation of Zn^{2+}, cathode materials must exhibit excellent structural stability and limited solubility. Quinone-based derivatives containing carbonyl groups have demonstrated strong coordination ability with Zn^{2+}, making them effective hosts for zinc storage. Nevertheless, the dissolution of redox intermediates or uncontrollable phase evolution often leads to limited cycle life. To address these issues, a thiophene-based organic quinone material (BNDTH) with multiple active functional groups and an extended π-conjugated framework was synthesized.[65] Despite these features, the material's practical performance was constrained by the low utilization of active sites and poor electrical conductivity. To overcome this, BNDTH was composited with reduced graphene oxide (RGO), which significantly improved conductivity and facilitated rapid charge transfer, thereby delivering a high specific capacity and excellent cycling performance (Fig. 6a).[65] In addition to carbonyl-based compounds, nitrogen-containing structures have also been identified as effective coordination sites for Zn^{2+}. In the discharge process of polyaniline cathodes, the reduced, non-protonated imine units (=N–) generate negatively charged nitrogen sites (–N–) that coordinate with Zn^{2+} (Fig. 6b).[66] Upon charging, Zn^{2+} is released via oxidation and rebinds with =N– groups, enabling reversible Zn^{2+} storage.

Recently, 2D conductive metal–organic frameworks (MOFs), such as Cu$_3$(HHTP)$_2$, have been introduced as cathode materials. Their high electrical conductivity and intrinsic porosity facilitate efficient charge and ion transport, leading to impressive performance with a capacity of 124.5 mAh g^{-1} at 4 A g^{-1} and a capacity retention of 75% at 0.5 A g^{-1}.[67] In parallel, covalent organic frameworks have also attracted increasing attention due to their designable architectures and tunable active sites. For example, a novel dual-active-center COF (TA-PTO-COF) achieved a specific capacity of 255 mAh g^{-1} at a current density of 0.1 A g^{-1}.[56] A key challenge for both MOF and COF materials lies in balancing high conductivity with structural robustness. For MOFs, enhancing active site utilization through doping or defect engineering is essential, whereas for COFs, optimizing interlayer interactions is crucial
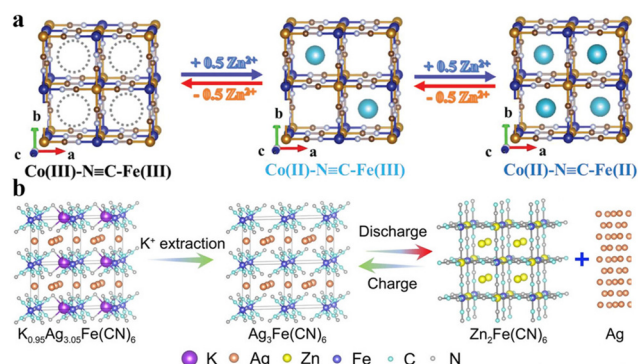
Fig. 5 (a) Schematic illustration of reversible Zn^{2+} intercalation/deintercalation in CoFe(CN)$_6$ frameworks during the electrochemical process. Reproduced with permission from ref. 62. (b) Schematic of the energy storage mechanism in AgHCF-3. Reproduced with permission from ref. 64.
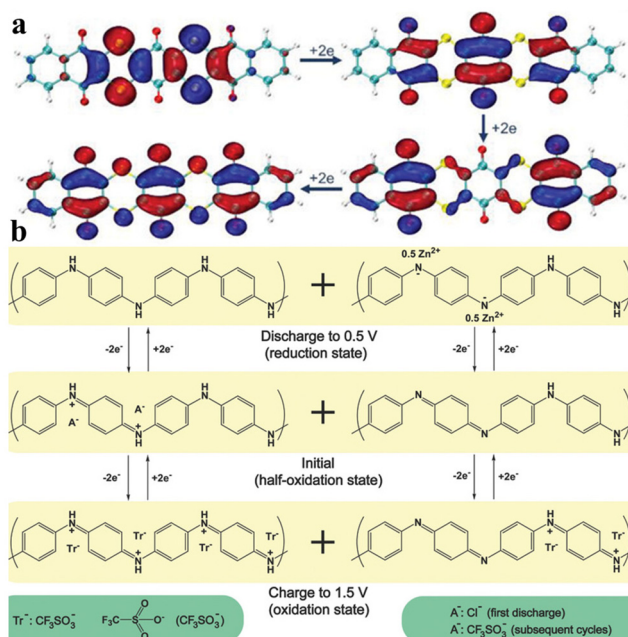
Fig. 6 (a) HOMO plots of selected molecules/anions with different extents of reduction of BNDTH. Reproduced with permission from ref. 65. (b) The proposed redox mechanism of PANI/CFs. Reproduced with permission from ref. 66.

to improving mechanical strength. Furthermore, the compatibility of these materials with the electrolyte system is vital. Designing low-concentration electrolytes with wide electrochemical windows may help suppress side reactions and reduce cost. Despite the progress achieved, further efforts are required to develop high performance organic electrode materials, thereby advancing the practical application of AZIBs.

4. Progress and overview of anode materials

In aqueous zinc electrodes, the cathode reaction varies depending on the type of material, and the reaction mechanism directly affects the performance and stability of the battery. For example, metal oxides such as V_2O_5 undergo typical embedding and de-embedding reactions, while organic molecules such as polyaniline and quinones undergo oxidation and reduction of reactive groups. In the broadly used weakly acidic electrolyte, the zinc anode reaction is considered to be a chemical reaction between Zn and Zn^{2+} in the electrolyte. In practice, dendrite growth and related side reactions at the zinc anode are two major problems. Zinc dendrite growth not only punctures the diaphragm and leads to short-circuiting of the battery but also increases the internal resistance of the battery and reduces the energy efficiency. Hydrogen evolution produces gas, leading to battery swelling and performance degradation. Corrosion and passivation reduce the activity of

the zinc anode, affecting the cycle life of the battery. These problems severely limit the cycling stability and practical application potential of AZIBs.

4.1 Challenges of the zinc anode

Among the key challenges, unavoidable dendrite growth is common in metal anodes based on deposition and dissolution reactions, and this phenomenon is particularly prominent in AZIBs. The uncontrollable growth of dendrites is prone to triggering internal short circuits in the battery leading to system failure.[68] Influenced by the weakly acidic electrolyte environment, the zinc deposition morphology usually shows unique mossy or flaky features. This contrasts with the typical dendritic morphology in alkali metal systems such as lithium and sodium.[69–71] Exploring the principle of zinc anode dendrite growth and then seeking an efficient solution is crucial for the wide application of AZIBs.

From a kinetic analysis, the electrodeposition process can be divided into three key stages (Fig. 7a).[72] Firstly, Zn^{2+} completes the diffusive migration in solution under the combined effect of the concentration gradient and the electric field force, and then Zn^{2+} ions migrating to the electrode surface are reduced to metallic zinc atoms through the charge transfer reaction. Finally, the zinc atoms in the reduced state undergo the nucleation and crystal growth process on the substrate surface.[73] It was found that the initial nucleation behaviour of zinc deposition has significant spatial selectivity, and the inherent crystal boundaries, dislocations, tips, and other highly active sites on the substrate surface preferentially adsorb Zn^{2+} and trigger the reduction reaction to form initial nucleation sites.[74] These initial nucleation sites, due to their lower nucleation barriers, further induce the preferential deposition of subsequent zinc atoms, ultimately leading to the directional growth of localized dendrites. As the electrodeposition continues, the Zn^{2+} concentration, substrate electric field distribution, and deposition rate in different regions become more and more different, which ultimately leads to inhomogeneous deposition and dendrite formation. This can also be seen in Fig. 7b.[75]

During the deposition process, when the substrate surface has a uniform microstructure, the electric field distribution is relatively uniform, which provides favourable conditions for the uniform deposition of Zn^{2+}. However, once a localized tip structure exists on the substrate surface, it leads to a significant enhancement of the electric field strength in that region, resulting in a localized electric field concentration that is much higher than that in other regions. This inhomogeneity of the electric field distribution increases as the deposition process proceeds. The tip region accelerates the deposition of Zn^{2+} due to the stronger electric field attraction, making the tip structure more and more obvious and further increasing the variability of the electric field distribution.

In addition to the dendrite problem, side reactions caused by water in the electrolyte can also degrade battery performance. Compared with the alkaline electrolyte, the weakly acidic electrolyte, which is widely used nowadays, has a higher
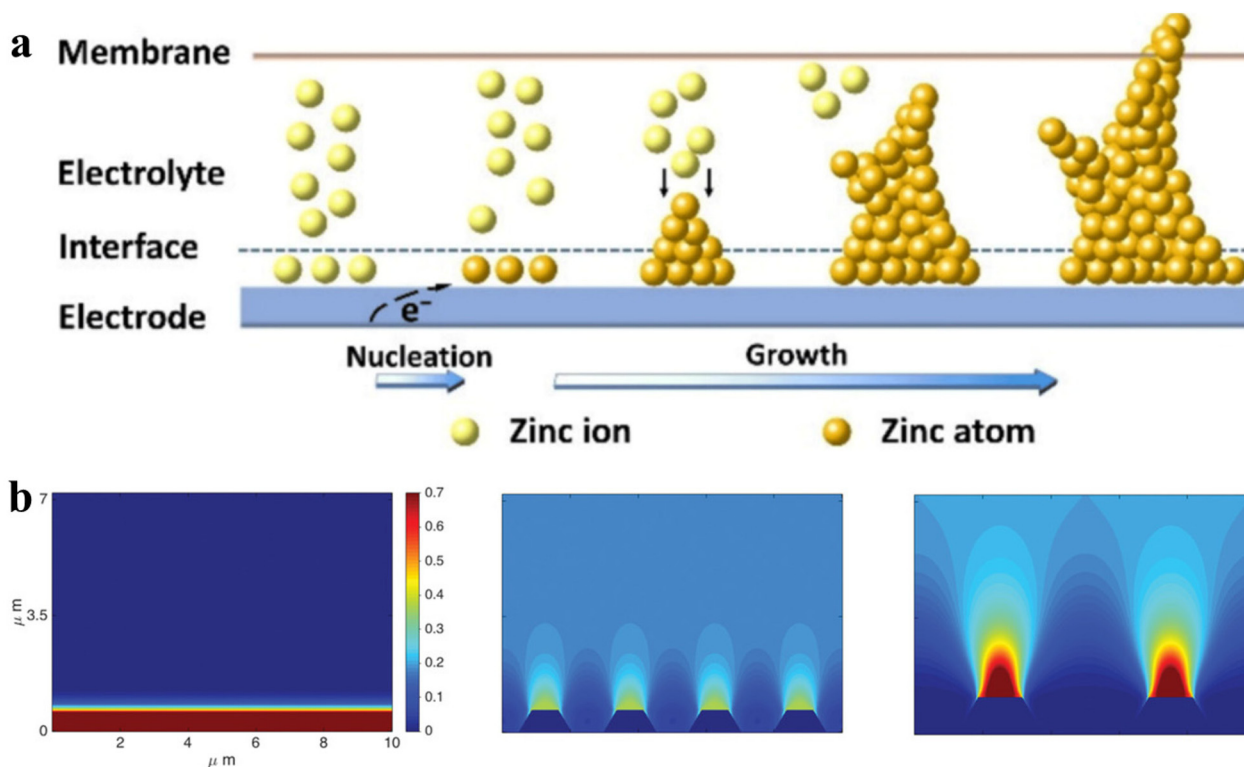
Fig. 7 (a) Schematic diagram of dendrite growth. Reproduced with permission from ref. 72. (b) COMSOL simulation of electric field distribution on the surface of substrates with different morphologies. Reproduced with permission from ref. 75.

thermodynamic tendency of the HER due to its higher proton activity. However, the interaction between hydrogen atoms adsorbed on the surface of the zinc metal anode and zinc is very weak, thus reducing the possibility of the HER.[76] Although thermodynamically favourable, it is kinetically much less efficient than zinc deposition. This is evident from the low exchange current density and high overpotential of the HER at the zinc anode surface, which also makes zinc deposition the dominant reaction actually observed, illustrating the important role of kinetic factors in electrochemical processes. Even if there is a relatively weak HER during the reaction, cumulative damage can still occur over time. Constant gas production can lead to cell expansion and eventually electrolyte leakage. Depletion of H^+ causes local pH changes, creating a locally alkaline environment.

The dendrite growth and side reactions of the zinc anode do not occur in isolation but form a cascading deterioration mechanism through the autocatalytic coupling effect. Specifically, the 3D growth of zinc anode dendrites significantly increases the specific surface area of the electrode, leading to the uneven distribution of the local current density, which accelerates the process of the HER. The OH^- will gradually increase the interface pH value and trigger the generation of the passivation layer. This not only aggravates the chemical corrosion of zinc but also leads to an exponential increase in the surface roughness of the electrode. The highly roughened interface further amplifies the electric field distortion through

the tip effect, providing a thermodynamic driving force for the preferential deposition of Zn^{2+}. This results in a vicious cycle of dendrite growth–HER–interface corrosion–dendrite growth. The establishment of this cascade reaction chain suggests a precise regulation strategy for the key links, and the above reactions can be effectively suppressed by rational design for any of the steps, thus improving the electrochemical performance. This provides an important theoretical basis for the design of high stability batteries.

4.2 Optimization strategies for artificial coatings

Based on the above analysis, realizing uniform deposition of Zn^{2+} and effectively suppressing the interfacial side reactions are the core keys to improve the electrochemical performance of the zinc anode. Researchers have carried out systematic exploration, focusing on the following innovative strategies: optimizing the ion transport path of the electrode through 3D structural design, developing a new electrolyte system to improve the electrochemical stability, constructing a multifunctional artificial interfacial coating to regulate the Zn^{2+} deposition behaviour, and functionalizing the diaphragm to inhibit the growth of dendrites. Among these approaches, the artificial coating technology has attracted much attention due to its multifunctionality. It can facilitate the ion desolvation process and accelerate the mass transfer kinetics. What is more, due to its easy preparation process and good potential for large scale production, the construction of functional coat-

ings directly on the surface of commercial zinc foils or zinc plates has become one of the most attractive strategies to enhance the performance of the zinc anode. Currently, diverse categories of coating material systems have been developed. As shown in Fig. 8, they mainly include inorganic materials (carbon-based materials, metals and their alloys, and inorganic compounds), organic materials (polymers, MOFs, COFs), and their composite systems, which provide a rich space for material selection for optimizing the performance of the zinc anode.[77]

4.2.1 Carbon-based materials. Carbon-based materials were initially used to increase the conductivity of the cathode, thereby improving the electrochemical performance of zinc electrodes.[78] On the anode side, carbon-based materials are also prevalent in the construction of functional artificial coatings due to their tunable structure, low cost, and non-toxicity.[79] In addition, carbon-based materials have good compatibility with AZIBs and remain stable in an aqueous solution environment. A wide range of specific carbon-based materials, including carbon fibers, carbon nanotubes, graphene, and activated carbon, can be used as coatings or substrates for zinc anodes. Acetylene black and activated carbon were combined with a binder to construct a functionalized protective layer on the surface of zinc foil by a coating process to achieve stabilization of the zinc anode. These methods can effectively improve the structural stability of the zinc anode by reducing the local current density and enhancing the mechanical strength. Although high viscosity binders can improve the mechanical properties of the coating, they inevitably reduce the electronic conductivity and ion transport capacity of the coating, which can adversely affect the interfacial charge transfer kinetics. This trade-off between electrical conductivity and mechanical properties is a key factor to focus on when optimizing the design of the protective layer for the zinc anode. A novel anode structure was developed by immersing a zinc plate into an ink containing carbon nanotubes, resulting in the formation of a

uniform carbon nanotube coating layer.[80] The special adsorption effect of carbon nanotubes helps to direct the side reactions to occur only on the coating, ensuring reversible deposition and stripping on the zinc foil. However, carbon-based materials lack sufficient zincophilicity, which plays an important role in improving the interfacial stability of the zinc anode. Nitrogen-doped carbon materials were synthesized and subsequently coated onto zinc foil to enhance the anode's electrochemical performance.[81] This coating gave the zinc anode a lower nucleation overpotential and higher corrosion resistance, and symmetric batteries assembled with this coating could be stably cycled for 800 h at 2 mA cm^{-2} and 2 mAh cm^{-2}.

4.2.2 Metals and alloys. Metals and alloys have been widely used in corrosion prevention due to their excellent electrical conductivity to protect the zinc anode from dendritic influences and side reactions. Typically, metals including Au,[23] Ag,[82] Cu,[83] Al,[84] and Sn[85] and alloys including Zn–Al[86] and Zn–Mn[87] have been reported to be used as the protective layer by *in situ* or *out-of-situ* preparation methods. The zincophilic Sb protective layer was successfully constructed on the surface of the zinc anode by the chemical replacement method.[88] Electrochemical impedance spectroscopy analysis revealed that the Zn@Sb anode exhibited a reduced charge transfer resistance. It was reduced by nearly 17 times compared to the unmodified electrode, and this result fully confirms that the Sb protective layer can effectively enhance the transfer kinetics performance of the electrode. To further evaluate the electrochemical performance, the researchers systematically tested the symmetric batteries using Zn@Sb electrodes at different current densities. Due to the abundant zincophilic sites provided by the Sb protective layer, the Zn@Sb anode exhibits lower voltage hysteresis and a more stable voltage plateau at all tested current densities, showing excellent rate performance and electrochemical stability.

4.2.3 Organic materials. Organic materials have superior chemical properties compared to a large number of inorganic materials. The ductility and flexibility of organic materials also facilitate the fabrication of more stable anode coatings. A generalized interphase strategy involving metal–organic complexes has been proposed to enable rapid and uniform zinc deposition, thereby significantly extending the lifespan of zinc-based batteries.[89] *In situ* complexation of a metal with phytic acid can build a zincophilic interface that kinetically homogenizes zinc nucleation and growth. The functional coating also protects the zinc anode from corrosion, and this ultrastable zinc anode has a dramatically improved coulombic efficiency during 800 cycles, with a cycle life of 4.25 Ah cm^{-2}. A structurally intact and defect-free zinc tartrate functional thin layer was successfully constructed on the surface of the zinc anode, providing enhanced interfacial stability and improved electrochemical performance.[90] This innovative surface modification method significantly accelerated the kinetic process of the layer-building reaction on the one hand, and effectively removed the adsorbed hydrogen molecules on the zinc surface on the other. It enables the zinc foil to fully undergo the re-
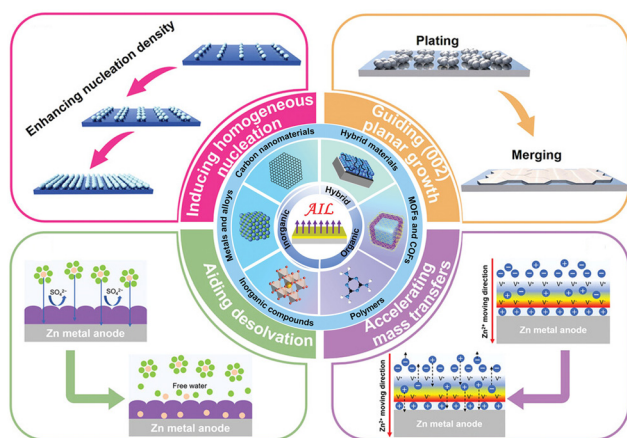
Fig. 8 Schematic illustration of AILs employing different types of material candidates and proposed functions in the realm of Zn anode protection. Reproduced with permission from ref. 77.

placement reaction with the tartaric acid solution, thus forming a uniformly dense and defect-free functional protective layer.

4.2.4 Natural polymers. Natural polymers, including cellulose, lignin, and proteins, have attracted attention for their sustainability and affordability. In the field of functionalized anodes, these polymers occupy an important position in anode coatings for AZIBs due to their polar groups that provide a large number of zincophilic sites. An ion-modified cellulose acetate functional coating combined with Zn $(CF_3SO_3)_2$ was innovatively constructed on the surface of the zinc anode, effectively enhancing interfacial stability and regulating zinc deposition behavior.[91] The coating exhibited excellent hydrophilic properties and significantly reduced the contact resistance at the interface, providing an efficient channel for ion transport. The C=O group in the coating was able to interact specifically with Zn^{2+}, and this unique intermolecular interaction could not only effectively regulate the deposition behaviour of ions, but also significantly promote the rapid diffusion process of ions, thus enhancing the kinetic performance of the electrode. The design of this multifunctional coating provides a new idea to improve the electrochemical performance of the zinc anode.

4.2.5 Synthetic polymers. Although natural polymers are abundant, synthetic polymers have emerged as highly promising materials for functionalizing zinc anodes, owing to their richer polar functional groups, tunable porous structures, and high chemical reactivity. Current research focuses on several core strategies: functional polymer coatings (*e.g.*, PDPTT rich in C=O and N groups),[92] highly porous framework materials (COFs, MOFs), and carbon dot (CD)-based interfacial engineering. Polymer coatings enriched with polar groups (such as C=O and N) can effectively coordinate with Zn^{2+}, promoting uniform zinc deposition and significantly suppressing dendrite formation. At the same time, they markedly lower the desolvation energy barrier of Zn^{2+} and improve reaction kinetics. Moreover, the interaction between these polar groups and the zinc substrate facilitates electron transfer, enhances the affinity between the anode surface and the electrolyte, further stabilizes the interface, and inhibits corrosion and other side reactions, thereby improving the overall cycling stability.

Highly porous framework materials provide deeper-level modification through precise structural design. Covalent organic framework (COF) films can be synthesized through interfacial reactions and are often coated in combination with polymers (such as PVDF) to enhance performance. The ordered channels of COFs can accurately regulate Zn^{2+} flux, guiding uniform deposition, while their structural flexibility helps accommodate the volume changes of zinc during charge/discharge.[93] Metal–organic framework (MOF) coatings (*e.g.*, zinc/copper composite MOF-ZCM) act directly as physical barriers, isolating the zinc anode from the electrolyte to fundamentally suppress interfacial side reactions.[94] The intrinsic high surface area, excellent electrolyte wettability, and chemical stability of MOFs provide abundant and uniformly distributed active sites for Zn^{2+} diffusion and deposition, working

synergistically to effectively inhibit the propagation of zinc dendrites.

As an emerging nanomaterial, carbon dots (CDs) feature a high specific surface area (with controllable sizes of 2–10 nm), excellent intrinsic conductivity (>100 S cm^{-1}), and tunable surface chemistry.[95] By dynamically forming a hydrophobic CD monolayer at the interface (or by trace addition to the electrolyte), CDs can reconstruct favorable hydrophobicity and electric double layer structure.[96] This reconstruction effectively suppresses water-dominated side reactions in the inner Helmholtz layer, while facilitating the desolvation of hydrated Zn^{2+} in the outer Helmholtz layer and reducing the desolvation energy barrier. Notably, this hydrophobic CD layer can maintain interfacial structural integrity during dynamic Zn^{2+} electrodeposition, achieving long-term protection of the zinc anode.

Compared to single organic or inorganic materials, composites exhibit superior performance through the synergistic effect of their components. This interaction between components not only realizes the complementary and enhanced functions but also expands the range of material choices for the zinc anode. The synergistic effect of different components in the composites can simultaneously optimize the mechanical strength, electrical conductivity, and interfacial stability, which provides a richer material system and a more flexible regulatory strategy for the design of high-performance zinc electrodes. A composite structure of carbon nanotubes (CNTs) was innovatively designed by modifying the ultra-thin nanocoating of α-In$_2$Se$_3$-Nafion (Fig. 9a), enabling enhanced surface functionality and performance.[97] Among them, α-In$_2$Se$_3$ nanosheets exhibited low nucleation barrier and strong affinity properties for Zn^{2+} by virtue of their unique crystal structure, which effectively optimized the nucleation behaviour of Zn. Meanwhile, the Nafion molecule can not only inhibit the participation of anions and free water molecules in the side reactions through its unique hydrophilic–hydrophobic region structure but also significantly enhance the mechanical flexibility of the interfacial layer. This bifunctional synergistic effect enabled the symmetric battery based on α-In$_2$Se$_3$-Nafion to cycle stably for 1500 h (Fig. 9b and c).[97]

4.3 Other optimization strategies

As part of the battery, the chemical composition of the electrolyte directly affects the ion diffusion behaviour and electrochemical reactions. Optimizing the electrolyte composition will have a favourable effect on the interfacial chemistry, thus improving the zinc anode performance. The concentration of the electrolyte determines its thermodynamic stability to some extent. The ZnCl$_2$ electrolyte potential window increases from 1.6 V (5 M ZnCl$_2$) to 2.3 V (30 M ZnCl$_2$) with increasing salt concentration.[98] As the zinc salt concentration increases, the water clusters decrease to their eventual disappearance. Due to the lack of water molecules in the high concentration electrolyte, the hydrated solvated structure strengthens the O–H bonds in the water molecules. Addition of another soluble salt to the electrolyte also disrupts the hydrogen bonding network
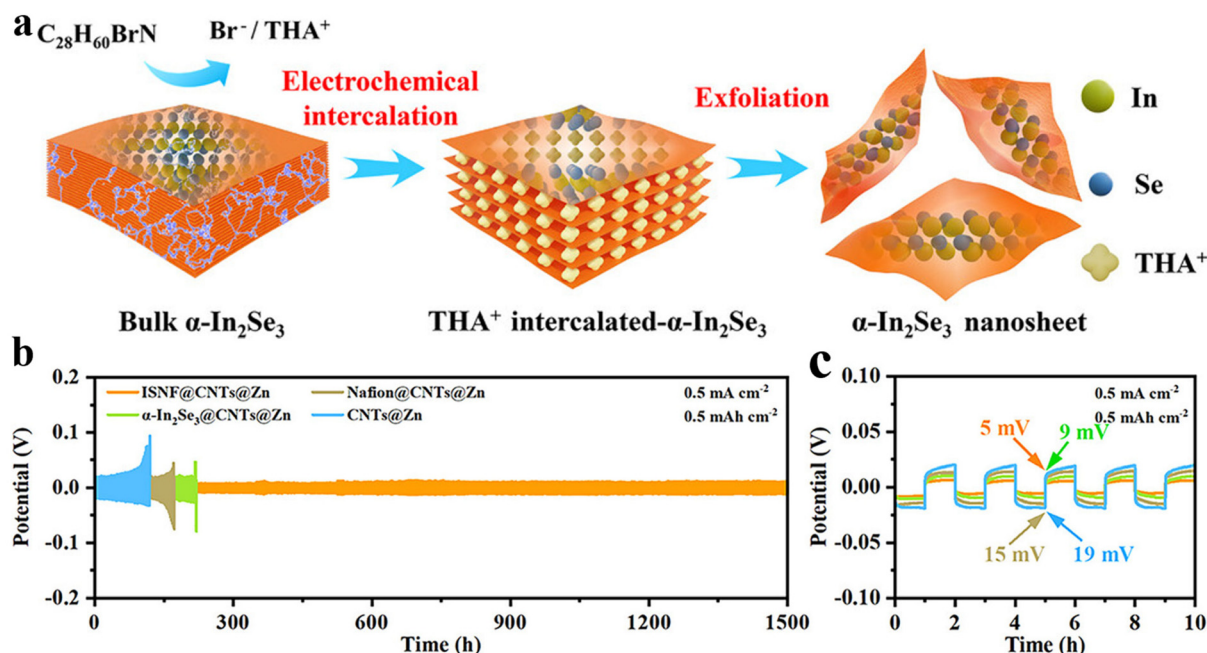
Fig. 9 (a) Schematic illustrations of fabricating α-In$_2$Se$_3$ nanosheets. Reproduced with permission from ref. 97. (b) Symmetric cells at 0.5 mA cm^{-2} for 0.5 mAh cm^{-2}. Reproduced with permission from ref. 97. (c) Magnified voltage–time curves. Reproduced with permission from ref. 97.

of the water clusters. The hydrated solvated structure of Zn^{2+} changes gradually with the increase of the soluble salt LiTFSI. In the dilute electrolyte of 1 M Zn(TFSI)$_2$ + 5 M LiTFSI, Zn^{2+} is coordinated to six water molecules.[99] Therefore, the deposition and stripping behaviour of Zn^{2+} can be regulated by modulating the salt concentration.

In the electrolyte of 1 M Zn(TFSI)$_2$ + 10 M LiTFSI, TFSI$^-$ replaced some of the original water molecules. When the concentration of LiTFSI was increased to 20 M, all six water molecules of the Zn^{2+} dissolution sheath were replaced by TFSI$^-$. An ultra-high-concentration NH$_4$Ac–NH$_3$–Zn(Ac)$_2$–Mn(Ac)$_2$ (46.5 M) electrolyte was developed, featuring dual metal complexation for Zn^{2+} and Mn^{2+} ions (Fig. 10a and b), effectively enhancing ion coordination and electrochemical performance.[100] Thus, the solvation effect of water molecules on Zn^{2+} and Mn^{2+} is greatly weakened. The full battery can be recycled 4500 times with a coulombic efficiency of 99%.

In addition to increasing the salt concentration, additives can be added to improve the thermodynamic stability of the electrolyte. A novel dual-additive hybrid electrolyte was developed by introducing trace amounts of mannose (DM) and sodium lignosulfonate (SLS) into the conventional ZnSO$_4$ electrolyte system, as illustrated in Fig. 10c.[101] The system takes full advantage of the significant difference in polarity between DM and LS^{2-}, enabling them to adsorb on the zinc metal surface in an alternating and parallel manner, forming a unique dynamic molecular phase. This molecular phase effectively modulates the Zn^{2+} flux during deposition and stripping, significantly inhibiting side reactions. When desorbed from the zinc surface, these additives were able to spontaneously enter the internal solvent sheath layer of Zn^{2+} due to their

thermodynamic properties, thus significantly improving the desorption kinetic process. This synergistic mechanism provides a new design idea for the development of high-performance aqueous electrolytes. Trace amounts of trisodium nitrilotriacetate (Na$_3$NTA) were introduced into the electrolyte to simultaneously optimize the solvated structure around Zn^{2+} and suppress the activity of water molecules, thereby ensuring stable battery cycling.[102]

Diaphragm, as an important component, plays a significant role in zinc deposition and stripping behaviour and battery performance. It is difficult for ordinary diaphragm materials to effectively inhibit the formation of an ion concentration gradient near the zinc anode due to the lack of ability to regulate the ion transport behaviour, which is the key trigger for zinc dendrite growth. The development of diaphragm materials with multifunctional properties has become an important research direction to improve the performance of the zinc anode. A functionalized nanofiber separator was successfully fabricated using an electrospinning technique combined with polydopamine surface modification and applied to AZIBs.[103] The diaphragm was designed with the following advantages. The abundant hydroxyl and amino functional groups on the surface of the diaphragm can form stable Zn–O and Zn–N coordination bonds with Zn^{2+}, which can effectively regulate the Zn^{2+} flux and promote its uniform deposition, thus inhibiting dendrites. The diaphragm significantly inhibits the shuttle effect of vanadium ions through the formation of V–O coordination bonds, providing effective protection for the anode. The capacity retention of the Zn–NH$_4$V$_4$O$_{10}$ battery with the functionalized diaphragm was as high as 92.3% after 1000 cycles at a high current density of 5 A g^{-1}. A dual-functionalized separa-
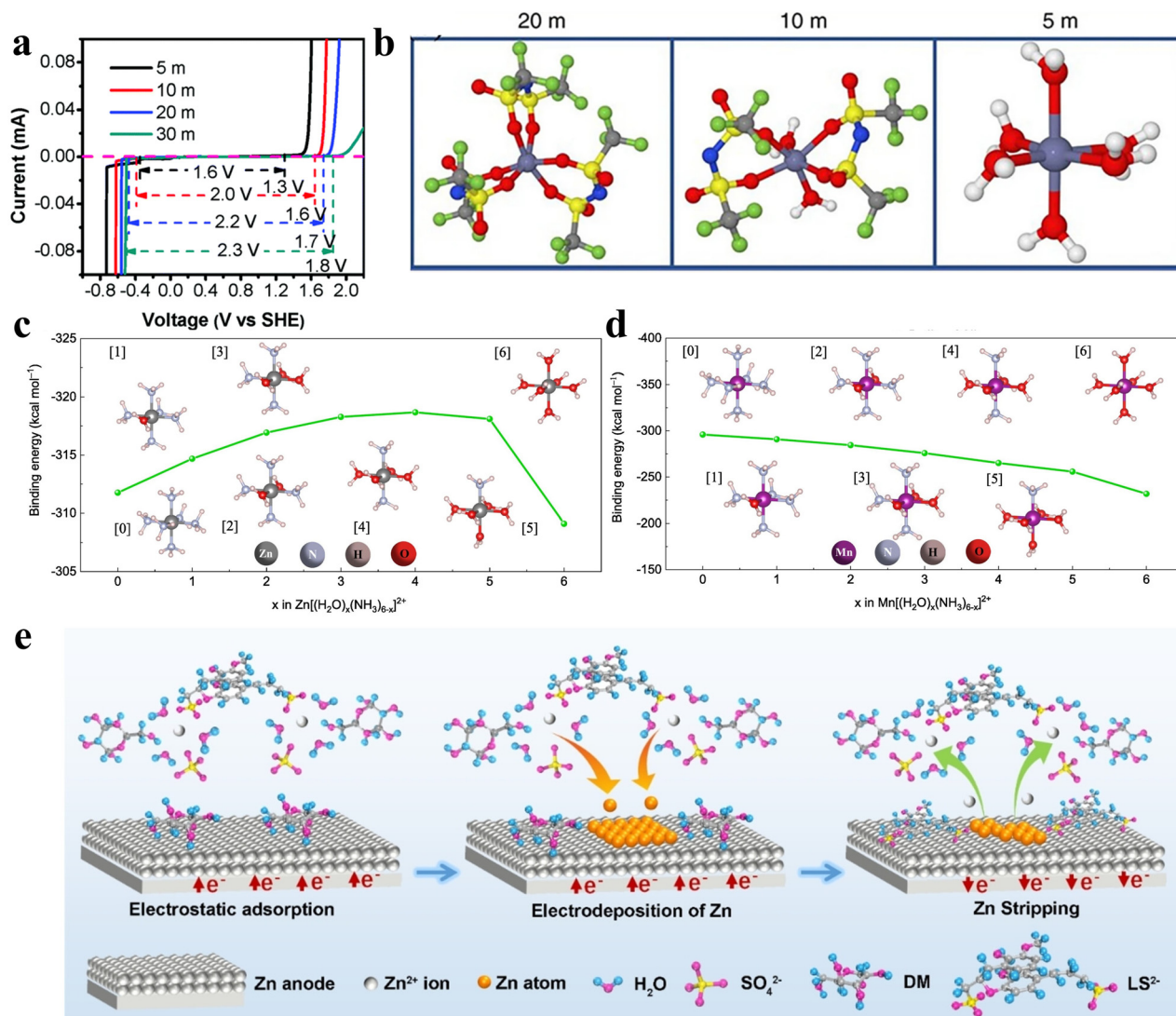
Fig. 10 (a and b) $Zn[(H_2O)_x(NH_3)_{6-x}]^{2+}$ and $Mn[(H_2O)_x(NH_3)_{6-x}]^{2+}$ complexes; the insets are molecular structure models with different coordination environments. Reproduced with permission from ref. 100. (c) Schematic illustration of the fabrication process of the PVDF@PDA separator. Reproduced with permission from ref. 101. (d) Schematics of the polyiodide absorption and conversion on polypropylene (PP), NrGO@PP, and Mo–rGO@PP separators. Reproduced with permission from ref. 104.

tor (Mo–rGO@PP) was successfully developed by anchoring molybdenum clusters on nitrogen and oxygen co-doped graphene nanosheets, followed by modification of a polypropylene separator (Fig. 10d). This innovative design effectively combines the advantages of both components to enhance battery performance.[104] The unique structure of this septum effectively promotes the redox reaction of polyiodides and significantly inhibits the shuttle effect of polyiodides. The introduction of molybdenum clusters enhanced the affinity of the diaphragm for ions and promoted its uniform deposition/exfoliation process. The battery assembled with this dual-functionalized diaphragm can be stably cycled at 10C for 6000 cycles.

Although conventional electrode materials have demonstrated promise in AZIBs, their practical deployment remains hindered by several critical challenges, including structural degradation of cathodes, sluggish ion diffusion, and severe interfacial side reactions.[105] To overcome these limitations and enhance battery performance, extensive efforts have been devoted to exploring novel electrode materials with tailored functionalities. In this context, MXenes, a rapidly expanding family of 2D transition metal carbides and nitrides, have garnered increasing attention in the energy storage community. Their unique characteristics, including a layered morphology, high electrical conductivity, tunable surface chemistry, and outstanding mechanical robustness, render them particularly attractive for AZIB applications. MXenes not only facilitate improved zinc-ion adsorption and diffusion kinetics *via* rational tuning of surface terminations but also function as multifunctional components, such as interfacial regulators or dendrite-suppressing coatings, capable of mitigating parasitic

reactions and enhancing electrochemical stability.[106] Furthermore, MXenes hold considerable promise in cathode engineering, where they can serve as conductive frameworks or hosts for active materials, promoting structural integrity and charge transport. The following sections detail the state-of-the-art in MXene research for AZIBs, including the history of development, synthesis approaches, structural design strategies, and emerging applications that showcase their versatility and performance-enhancing capabilities.[107]

5. Advances in MXene materials research

5.1 History of development

MXenes are obtained by selective etching of A-metal elements in the MAX phase, which are a ternary carbide or nitride with a layered hexagonal structure and the general formula of $M_{n+1}AX_n$, where M stands for transition metals (Ti, Nb, Cr, Mo), A represents the main group elements, X represents C or N, and $n = 1, 2, 3$ (Fig. 11).[108,109] After etching out the element A, the $n + 1$ layers of M are interspersed with the n layers of X, and thus the general formula of MXenes is $M_{n+1}X_nT_x$, where T_x represents the surface end groups (–O, –OH, –F, –Cl). The creation of MXenes further expanded 2D inorganic materials, including $Ti_3C_2T_x$, V_2CT_x, and Nb_2CT_x. In recent years, significant progress has been made in the study of MXene materials, and 46 MXene materials have been successfully synthesized and characterized.[110] Theoretical predictions based on first principles calculations indicate that there are still a large number of MXene candidates with potential applications that need to be exploited, and MXene materials have shown great potential for applications in several frontier fields by virtue of their excellent intrinsic electrical conductivity, regular layered structure, and high specific surface area. MXene materials not only cover basic research in materials science but also extend to photovoltaic devices, energy storage systems, supercapacitors, water treatment, catalysis, and biomedicine. MXene materials provide abundant active sites at the end groups, which is a structural feature that enables them to exhibit more excellent catalytic performance than traditional 2D materials with catalytic activity at the edge of the sites, providing a new way to develop new types of materials.

5.2 Preparation methods

The preparation of MXene materials is mainly based on the structural transformation process of MAX phase precursors. MAX, as a typical 3D layered material, can be transformed into MXenes with a 2D layered structure through a specific etching process. Currently, the preparation methods of MXenes are mainly categorized into top-down and bottom-up. The top-down method involves selective removal of A-layer atoms in the MAX phase by chemical etching, followed by a peeling process to obtain monolayer MXene nanosheets. The bottom-up approach allows direct synthesis of MXene materials without the MAX phase etching step. The MXene materials produced by this method have the advantages of large size and few defects. Among the many preparation methods, the top-down method is currently the most widely used preparation strategy due to its mature and controllable process. The methods mainly include hydrofluoric acid (HF) etching, *in situ* HF etching, molten salt etching, and electrochemical etching. Each of these methods has its own characteristics, providing diverse technical paths for the controllable preparation of MXenes.

The typical method of synthesis is HF etching. Naguib first proposed the use of HF for etching.[111] After immersing the MAX powder in a certain concentration of aqueous HF and stirring for a certain period of time at room temperature, the solid is separated from the supernatant by centrifugation or filtration, and then washed with deionized water until the suspension is weakly acidic, and finally the solid is dried to obtain the MXene powder. The reaction equation is as follows:

$$M_{n+1}AlX_n + 3HF \rightarrow AlF_3 + 1.5H_2 \uparrow + M_{n+1}X_n \quad (5)$$
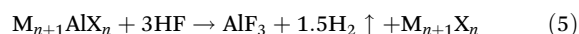
Due to the harmful effects of HF, researchers are working on finding ways to avoid the direct use of HF in the etching process. A hybrid etching method based on lithium fluoride (LiF) and hydrochloric acid (HCl) was developed.[112] In this method, 1.6 g of LiF was mixed with 20 ml of 9 M HCl. Then, 1.0 g of Ti_3AlC_2 powder was added to the solution and reacted at 40 °C for 24 h. After etching, it was washed repeatedly with deionized water until neutral. Finally, the product was sonicated under inert gas flow to obtain $Ti_3C_2T_x$ MXene suspension. The MXene material produced by this method exhibits excellent hydrophilic properties, and it can undergo significant volume expansion during the water washing process to exhibit special clay-like properties. The clay film exhibits excellent
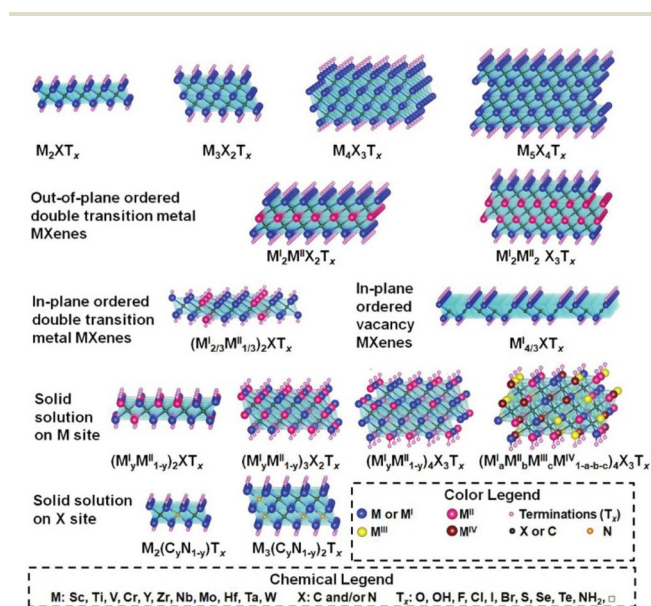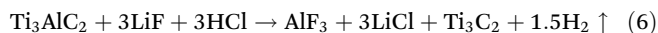

Fig. 11 Typical MXene structures and compositions. Reproduced with permission from ref. 109.

electrochemical properties, and this innovative preparation method provides a new technological approach for the large-scale production and application of MXene materials. The reaction equation is as follows:

$$Ti_3AlC_2 + 3LiF + 3HCl \rightarrow AlF_3 + 3LiCl + Ti_3C_2 + 1.5H_2 \uparrow \quad (6)$$

On the basis of significant progress in MXene materials research, Gogotsi and colleagues were the first to realize the breakthrough synthesis of $Ti_4N_3T_x$.[113] Unlike the traditional acidic etching solution, the team innovatively used the molten fluoride salt etching method (LiF, NaF, KF) to successfully selectively remove the Al atomic layer from Ti_4AlN_3 phase powder under argon protection at 550 °C, thus obtaining $Ti_4N_3T_x$ MXenes. This novel research method provides a new way to prepare MXenes. The molten salt etching technique was further optimized using a $ZnCl_2$-based system, successfully preparing various Zn-containing MAX phase precursors. Through this approach, $Ti_3C_2Cl_2$ and Ti_2CCl_2 MXenes were obtained by direct exfoliation in molten salt, demonstrating an effective method for MXene synthesis with controlled composition and surface termination.[114] The reaction equations are as follows:

$$Ti_3AlC_2 + 1.5ZnCl_2 \rightarrow AlCl_3 + Ti_3ZnC_2 + 0.5Zn \quad (7)$$
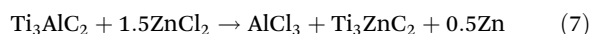
Most etching methods rely on an etchant, but an etchant can affect the etching effect to some extent.[115] In the absence of an etchant, electrochemical etching can reduce the undesirable effects of the etchant. The Ti_3C_2 MXene was successfully synthesized *via* electrochemical etching of porous Ti_3AlC_2 electrodes in NH_4HF_2 solution, clearly revealing the reaction mechanism and voltage-dependent etching behaviour. This method enabled precise surface functionalization control while preserving structural integrity.[116] $Ti_3C_2T_x$ was prepared by electrochemical etching of porous Ti_3AlC_2 sheet electrodes in a solution comprising NH_4Cl and TMAOH. The reaction equation is given below:

$$Ti_3AlC_2 - 3e^- + 3Cl^- \rightarrow Ti_3C_2 + AlCl_3 \quad (8)$$
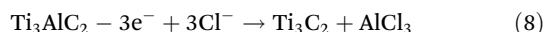
In addition to the traditional top-down preparation methods, the synthesis strategies of MXenes have also been expanding. A fused copper-catalysed chemical vapor deposition method was developed based on molten copper catalysis, achieving the direct one-step synthesis of MXenes. This innovative approach leveraged the catalytic properties of molten copper to enable efficient and scalable MXene production.[117] Due to the unique interfacial charge transfer kinetics, the Mo_2C MXene materials prepared by this method exhibited significantly better electrocatalytic activity in the HER than the Mo_2C MXene catalysts synthesized by conventional methods. A simple and efficient topochemical pyrolysis method was developed, which innovatively employed Fe-Pc as the precursor while incorporating an ionic liquid as a partial carbon source. This approach enabled precise control over the pyrolysis process while enhancing the material's structural properties. The two synergistically formed a self-templated

system, and quasi-MXene materials with stacked-layer structures were successfully constructed through topological transformations.[118] This novel structure not only exhibits excellent electrochemical performance but also shows outstanding cycling stability.

5.3 Application in aqueous zinc-ion batteries

MXenes, as an emerging class of 2D materials, show great potential for application in the field of aqueous zinc electrodes by virtue of their unique physicochemical properties. Their excellent mechanical strength, outstanding electrical conductivity, rich surface functional groups, and tunable layered structure provide multiple advantages for optimizing the electrochemical performance of batteries. As important materials in the current energy field, the application of MXenes in zinc electrodes has made significant progress, including breakthroughs in enhancing the electrical conductivity of electrode materials, optimizing the ion transport kinetics, and enhancing the structural stability, which provides a new research direction for the development of the next generation of high-performance zinc electrodes.

Although the 2D MXene materials prepared by the etching method exhibit many excellent properties, there are still obvious structural defects. Due to the presence of surface functional groups, the surface activity of MXenes is significantly enhanced, and uncontrollable stacking between the lamellae is prone to occur. This not only limits the fast ion transport but also affects the electrochemical performance of the material. To address this problem, researchers developed an effective strategy for intercalation modification. By introducing intercalators such as ions, organic molecules, or polymers, the interlayer spacing of MXenes can be significantly enlarged to effectively alleviate the lamellar stacking problem. Experiments have confirmed that this intercalation modification method not only improves the structural properties of MXenes but also significantly enhances their alkali metal ion storage capacity, which provides a reliable technological pathway to optimize the electrochemical performance of MXenes.

5.3.1 Application of MXenes in cathode materials. Bimbo developed a novel intercalation strategy by introducing a surfactant as a functional additive to achieve the precise modulation of the electrode structure of MXenes.[119] Kinetic analysis and spectroscopic characterization revealed that the embedding and de-embedding behaviour of Zn^{2+} is characterized by a dual mechanism, which involves both surface-dominated pseudo-capacitive processes and battery-like redox processes embedded in the bulk phase. This breakthrough discovery confirms for the first time in an aqueous multivalent ion energy storage system that MXenes can achieve charge storage *via* a Faraday redox mechanism. The *in situ* intercalation strategy can regulate the layer spacing of MXenes, which not only significantly enhances the pseudo capacitance of the material but also effectively suppresses the bulk deformation during cycling through the stress-buffering effect. Due to this synergistic optimization mechanism, the capacity retention rate of

the constructed battery is still as high as 96.2% after 1000 cycles.

The expansion of the layer spacing can only promote ion diffusion but not shorten the ion transport path. A vertical array structure of the Sn^{4+} pre-intercalated Ti_2CT_x MXene was developed (Fig. 12a).[120] The MXene nanosheets were arranged in a radial order on the surface of carbon spheres, and the Sn^{4+} pre-intercalation layer effectively eliminated the surface barriers and reduced the ion transport resistance. The spacing of the MXene layers was extended from the initial 1.3 nm to 1.8 nm, which provided a smoother diffusion channel for Zn^{2+}. The vertical array structure significantly shortens the ion diffusion path (<50 nm), which greatly enhances the reaction kinetics. Due to these structural advantages, the constructed Zn-MXene capacitor has a high-capacity retention rate of 98.5% after 12 500 cycles at 5 A g^{-1}.

5.3.2 Application of MXenes in anode materials. In addition to being used as cathode materials, MXenes are also considered to be good anode materials. This is due to not only their inherent excellent properties but also their surface-tunable terminal groups and their ability to synergize with other materials to optimize zinc anode performance. There are various ways to obtain MXenes by etching, and different end groups can be introduced in different etching environments. These end groups not only change the lattice constant, nucleation energy barrier, and conductivity of the sample but also significantly affect the adsorption energy. An *in situ* self-assem-

bly strategy was developed to construct an ultrathin and uniform MXene protective layer on the surface of the zinc anode (Fig. 12b).[121] The theoretical basis of this method lies in the fact that the reduction potential of the oxygen-containing terminal groups of MXenes is significantly higher than that of Zn^{2+}, which enables the zinc foil to spontaneously reduce the MXene nanosheets. The experimental procedure consists of immersing the zinc foil into a homogeneously dispersed MXene colloidal solution, where ionization occurs on the surface of the zinc foil and the released electrons are rapidly transferred to the surface of the MXene nanosheets. Meanwhile, the Zn^{2+} generated at the interface interacts with the negatively charged oxygen-containing functional groups on the surface of the MXene nanosheets to further promote the reduction process of MXenes. The assembled symmetric battery achieved a long cycle life, and the capacity retention rate of the full battery was as high as 81% after 500 cycles.

A hierarchical interfacial layer of the N/Se-doped MXene–ZnSe composite was *in situ* generated on zinc foil surfaces through a one-step vacuum heat treatment (Fig. 12c).[122] The hierarchical structure of N/Se-functionalized and crumpled MXene nanosheets can improve hydrophilicity, provide sufficient electron channels, regulate uniform electric field distribution, adapt to the volume change, and act as a physical barrier. Meanwhile, the synchronized formation of ZnSe nanoparticles at 350 °C can provide sufficient zincophilic sites for uniform Zn^{2+} distribution, reduce overpotential and improve reversibility with a cycling life of up to 2500 h. To further optimize the structure and performance of MXenes, a Lewis salt etching strategy was proposed.[123] MXene materials were successfully prepared with a highly matched zinc lattice by precisely tuning the etching conditions. This lattice-matching-induced synergistic effect effectively guided Zn^{2+} to nucleate uniformly and realize planar-like optimal growth on the (000L) crystal surface of the MXene substrate, which provides a new technological pathway for the development of high-performance zinc-based energy storage devices.

5.3.3 Application of MXenes in diaphragms and electrolytes. In addition to its application in electrodes, MXenes are also widely used in diaphragms and electrolytes. The $Ti_3C_2T_x$ MXene was initially employed as an electrolyte additive in zinc-based systems, where it facilitated controlled Zn^{2+} plating and stripping behaviors. This innovative approach demonstrated remarkable effectiveness in controlling Zn^{2+} behaviour while maintaining electrochemical stability. The electrolyte system with the MXene additive achieved dendrite-free Zn^{2+} deposition and stripping behaviour and exhibited excellent electrochemical performance. The coulombic efficiency was as high as 99.7% at 2 mA cm^{-2} and excellent reversibility was maintained over 1180 cycles. The $Ti_3C_2T_x$ MXene was first introduced as an electrolyte additive in zinc electrode systems, achieving precise regulation of Zn^{2+} deposition and stripping behaviour. This novel strategy enabled regulated Zn^{2+} migration without compromising electrochemical stability.[124] The optimized diaphragm exhibits a significantly higher dielectric constant compared to commercial
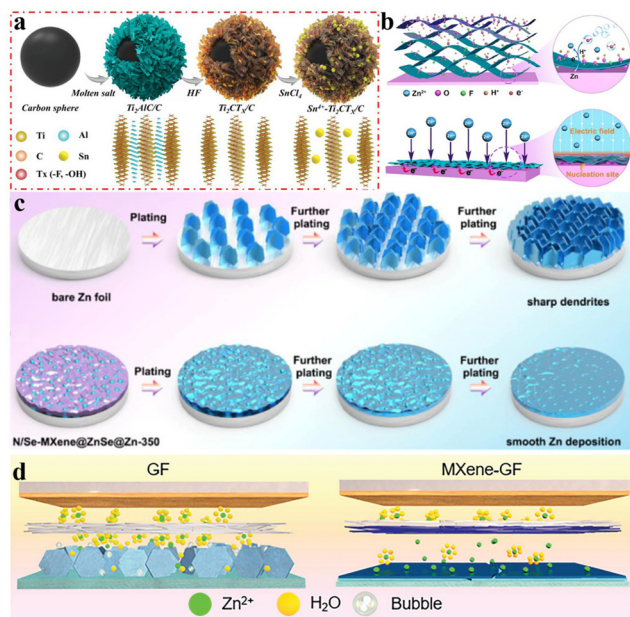
Fig. 12 (a) Schematic illustration of the preparation process of the core–shell Sn^{4+}–Ti_2CT_x/C sphere. Reproduced with permission from ref. 120. (b) Illustration of the synchronously reducing and assembling MXene layer on the surface of Zn foil. Reproduced with permission from ref. 121. (c) The schematic illustration of Zn deposition behaviours. Reproduced with permission from ref. 122. (d) Schematic representation of AZIB full cells equipped with GF or MXene–GF as the separator. Reproduced with permission from ref. 124.
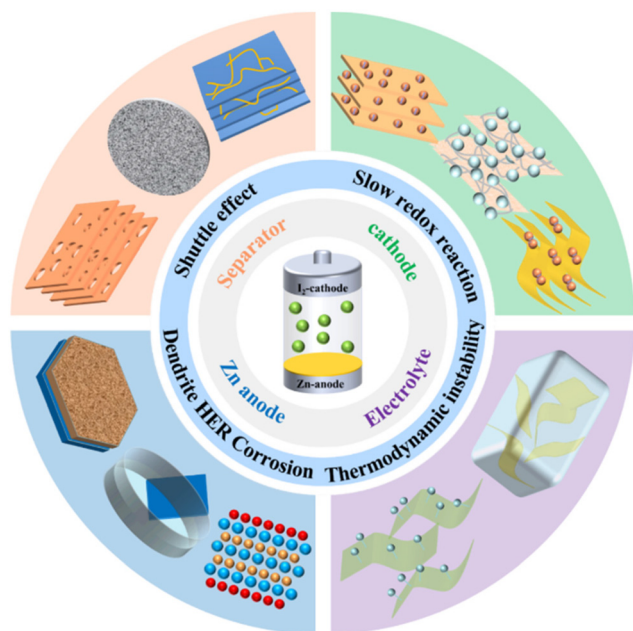
Fig. 13 Schematic representation of the modification of MXenes and the optimization strategy for solving AZIBs.

diaphragms. This property accelerates the migration process of Zn^{2+} by constructing a uniform built-in electric field at the electrode–electrolyte interface through the Maxwell–Wagner effect, thus inhibiting the growth of dendrites at the kinetic level (Fig. 12d).[124] The symmetric cell assembled with MXene–glass fiber (GF) achieved a cycle life of 1180 h under test conditions of 1 mA cm^{-2} and 1 mAh cm^{-2}.

5.3.4 Conclusion. In summary, as emerging 2D materials, MXenes exhibit significant application potential in AZIBs owing to their high electrical conductivity, tunable interlayer spacing, abundant surface functional groups, and excellent hydrophilicity.[14] As illustrated in Fig. 13, we systematically summarize the key roles of MXenes in AZIBs when employed as a cathode, anode, separator, and electrolyte additive, along with the corresponding functionalization strategies and their impacts on battery performance. These studies clearly demonstrate the versatile regulatory effects of MXenes in AZIBs, offering new insights and material platforms for the development of high-performance and long-life aqueous zinc-ion batteries.[125]

6. Summary and outlook

Aqueous zinc-ion batteries (AZIBs) have emerged as a promising candidate for next-generation energy storage systems, offering key advantages such as high intrinsic safety, environmental compatibility, and cost-effectiveness. Despite this potential, several critical challenges continue to hinder their practical deployment, including cathode structural instability, sluggish ion diffusion kinetics, and severe interfacial side reactions. Addressing these issues is essential for realizing the full potential of AZIBs in real-world applications. This review

begins by providing a comprehensive overview of the charge storage mechanisms in zinc-ion batteries, followed by a detailed discussion on the development of zinc and cathode materials. Among the various material strategies explored, MXenes have emerged as a particularly attractive class of two-dimensional materials. Their high electrical conductivity, mechanical flexibility, tunable surface chemistry, and excellent hydrophilicity make them highly suitable for engineering stable electrode/electrolyte interfaces, reinforcing structural integrity, and enhancing electrochemical reversibility. Through a range of engineering strategies, including surface functionalization, interlayer extension, and construction of heterogeneous structures, MXenes have demonstrated their ability to inhibit dendrite growth, reduce parasitic reactions, and promote uniform deposition of Zn^{2+}. This review systematically outlines the historical development and fundamental electrochemical principles of AZIBs, summarizes progress in electrode materials, and emphasizes the synthesis techniques, material properties, and functional applications of MXenes within this context. In addition, the review provides an in-depth discussion of various MXene modification strategies, such as organic intercalation, heterogeneous surface design, and surface chemical modulation, and elucidates their roles in improving electrochemical performance. By integrating and analyzing these approaches, this review not only clarifies the mechanistic insights behind MXene-enabled improvements but also offers valuable guidance for future material design.

Despite these advances, several fundamental aspects warrant deeper investigation to unlock the full potential of MXenes in energy storage applications. One of the most pressing challenges lies in improving the intrinsic electrochemical activity of MXenes when directly employed as cathode materials. Their typically limited specific capacity and insufficient cycling stability arise from restricted redox-active sites and ion diffusion confined by interlayer spacing. To overcome these constraints, future work must explore rational structural tuning, such as interlayer chemistry engineering, functional group modulation, and electronic band structure optimization, with the aim of activating more reversible redox processes and ensuring long-term operational stability. Beyond structural refinement, the compositional diversity of MXenes remains a largely untapped resource. Most studies to date have centered on $Ti_3C_2T_x$, derived from Ti_3AlC_2 MAX phases, while a broad spectrum of alternative precursors, including V_2AlC, Nb_2AlC, and Mo_2Ga_2C, offer opportunities for tailoring electronic configuration, ion transport characteristics, and surface reactivity. However, the synthesis of these variants is often limited by harsh chemical etching procedures and poor scalability. Advancing green, controllable, and scalable synthesis approaches will be critical to expanding the MXene family and discovering novel compositions with unique electrochemical signatures.

In addition to functioning as electrode materials, MXenes are beginning to show promise as dynamic electrolyte additives. Their incorporation into electrolytes has been shown to influence ionic conductivity, suppress side reactions, and stabilize Zn^{2+} solvation structures, suggesting a broader role in

interfacial modulation. Nonetheless, the fundamental nature of the interactions between MXenes and solvent or solute species remains poorly understood. Comprehensive *in situ* and theoretical studies are needed to elucidate these interfacial phenomena, which could inform the rational design of next-generation electrolytes that synergize with MXene surfaces. Moreover, the utility of MXenes is not confined to AZIBs. Their high surface area, strong metal affinity, and ionic transport tunability make them attractive candidates for broader classes of energy storage devices, including sodium-ion, lithium-ion, magnesium-ion, and aluminum-ion batteries. These multi-valent systems often face similar challenges to AZIBs, such as dendrite growth, sluggish charge transfer, and structural breakdown. The adaptation of MXenes to these systems could provide generalizable solutions through interface stabilization, dendrite suppression, and enhancement of ion mobility.

In conclusion, while MXenes have already demonstrated substantial promise in addressing key limitations of AZIBs, the next stage of development will depend on deepening our fundamental understanding of their structure–property–function relationships across multiple battery components. By employing high-resolution *in situ* characterization techniques (such as *in situ* electron microscopy and synchrotron spectroscopy), it is possible to track in real time the microscopic evolution of MXenes in their multiple roles – as electrodes, interfacial modification layers, and functional separators – under battery operating conditions, and to uncover their interfacial symbiosis mechanisms with electrolytes and zinc anodes, which is key to unlocking the material's fundamental functionalities. Furthermore, integrating AI-driven multi-scale simulations (*e.g.*, machine-learning potentials and high-throughput calculations) with big data mining can accurately predict the performance landscape of novel MXene heterostructures, surface termination engineering, and single-atom modifications, thereby guiding targeted experimental designs for validation. Unlocking new compositions, exploring multifunctional roles, and designing integrated MXene-based architectures will be pivotal in advancing not only zinc-ion batteries but also a broader spectrum of sustainable energy storage technologies.

Author contributions

J. L. and J. Z. wrote the manuscript; all authors have given approval to the final version of the manuscript.

Conflicts of interest

The authors declare no conflict of interest.

Data availability

The data that support the findings of this study are available from the corresponding author upon reasonable request.

Acknowledgements

References

1 J.-Y. Hwang, S.-T. Myung and Y.-K. Sun, *Chem. Soc. Rev.*, 2017, **46**, 3529–3614.

2 Y.-X. Yao, L. Xu, C. Yan and Q. Zhang, *EES Batteries*, 2025, **1**, 1–22.

3 X. Wang, G. Pawar, Y. Li, X. Ren, M. Zhang, B. Lu, A. Banerjee, P. Liu, E. J. Dufek, J.-G. Zhang, J. Xiao, J. Liu, Y. S. Meng and B. Liaw, *Nat. Mater.*, 2020, **19**, 1339–1345.

4 F. Wan, X. Zhou, Y. Lu, Z. Niu and J. Chen, *ACS Energy Lett.*, 2020, **5**, 3569–3590.

5 X. Wang, Z. Zhang, B. Xi, W. Chen, Y. Jia, J. Feng and S. Xiong, *ACS Nano*, 2021, **15**, 9244–9272.

6 X. Chen, W. Li, D. Reed, X. Li and X. Liu, *Electrochem. Energy Rev.*, 2023, **6**, 33.

7 G. Liu, Y. Tang, H. Li, J. He, M. Ye, Y. Zhang, Z. Wen, X. Liu and C. C. Li, *Angew. Chem., Int. Ed.*, 2023, **62**, e202217945.

8 F. Zeng, S. Li, S. Hu, M. Qiu, G. Zhang, M. Li, C. Chang, H. Wang, M. Xu, L. Zheng, Y. Tang, C. Han and H. M. Cheng, *Adv. Funct. Mater.*, 2024, **34**, 2302397.

9 B. Liu, T. Lv, A. Zhou, X. Zhu, Z. Lin, T. Lin and L. Suo, *Nat. Commun.*, 2024, **15**, 2922.

10 Q. Lin, Z. Jinqiu, S. Meizhu, Y. Xiuzhen, S. Xiaowei, Y. Chenglin and Q. Tao, *Energy Storage Mater.*, 2025, **74**, 103917.

11 W. Du, E. H. Ang, Y. Yang, Y. Zhang, M. Ye and C. C. Li, *Energy Environ. Sci.*, 2020, **13**, 3330–3360.

12 Z. Yi, G. Chen, F. Hou, L. Wang and J. Liang, *Adv. Energy Mater.*, 2021, **11**, 2003065.

13 J. Hao, S. Zhang, H. Wu, L. Yuan, K. Davey and S.-Z. Qiao, *Chem. Soc. Rev.*, 2024, **53**, 4312–4332.

14 R. Jia, R. Yang, Y. Zheng, Q. Pan, F. Zhang and Y. Tang, *Adv. Funct. Mater.*, 2025, **35**, 2419013.

15 C. Bao, J. Wang, B. Wang, J. Sun, L. He, Z. Pan, Y. Jiang, D. Wang, X. Liu, S. X. Dou and J. Wang, *ACS Nano*, 2022, **16**, 17197–17209.

16 F. Song, J. Hu, G. Li, J. Wang, S. Chen, X. Xie, Z. Wu and N. Zhang, *Nano–Micro Lett.*, 2021, **14**, 37.

17 Z. Cai, J. Wang and Y. Sun, *eScience*, 2023, **3**, 100093.

18 K. Du, Y. Liu, Y. Yang, F. Cui, J. Wang, M. Han, J. Su, J. Wang, X. Han and Y. Hu, *Adv. Mater.*, 2023, **35**, 2301538.

19 Y. Shi, Y. Chen, L. Shi, K. Wang, B. Wang, L. Li, Y. Ma, Y. Li, Z. Sun, W. Ali and S. Ding, *Small*, 2020, **16**, 2000730.

20 H. Chen, X. Li, K. Fang, H. Wang, J. Ning and Y. Hu, *Adv. Energy Mater.*, 2023, **13**, 2302187.

21 A. Ivette, B. John, G. Louis, D. Florian, B. Véronique, K. Frédéric and T. Jean-Marie, *Joule*, 2025, **9**, 101784.

22 C. Xu, B. Li, H. Du and F. Kang, *Angew. Chem., Int. Ed.*, 2012, **51**, 933–935.

23 H. Li, L. Ma, C. Han, Z. Wang, Z. Liu, Z. Tang and C. Zhi, *Nano Energy*, 2019, **62**, 550–587.

24 J. R. Loh, J. Xue and W. S. V. Lee, *Small Methods*, 2023, **7**, 2300101.

25 M. Zhang, X. Zhang, Q. Dong, S. Zhang, Z. Xu, Z. Hou and Y. Qian, *Adv. Funct. Mater.*, 2023, **33**, 2213187.

26 K. W. Nam, H. Kim, J. H. Choi and J. W. Choi, *Energy Environ. Sci.*, 2019, **12**, 1999–2009.

27 M. H. Alfaruqi, V. Mathew, J. Gim, S. Kim, J. Song, J. P. Baboo, S. H. Choi and J. Kim, *Chem. Mater.*, 2015, **27**, 3609–3620.

28 C. Wei, C. Xu, B. Li, H. Du and F. Kang, *J. Phys. Chem. Solids*, 2012, **73**, 1487–1491.

29 S. Li, C. Huang, L. Gao, Q. Shen, P. Li, X. Qu, L. Jiao and Y. Liu, *Angew. Chem., Int. Ed.*, 2022, **61**, e202211478.

30 M. Wu, C. Shi, J. Yang, Y. Zong, Y. Chen, Z. Ren, Y. Zhao, Z. Li, W. Zhang, L. Wang, X. Huang, W. Wen, X. Li, X. Ning, X. Ren and D. Zhu, *Adv. Mater.*, 2024, **36**, 2310434.

31 D. Kundu, B. D. Adams, V. Duffort, S. H. Vajargah and L. F. Nazar, *Nat. Energy*, 2016, **1**, 16119.

32 H. Pan, Y. Shao, P. Yan, Y. Cheng, K. S. Han, Z. Nie, C. Wang, J. Yang, X. Li, P. Bhattacharya, K. T. Mueller and J. Liu, *Nat. Energy*, 2016, **1**, 16039.

33 W. Liu, X. Zhang, Y. Huang, B. Jiang, Z. Chang, C. Xu and F. Kang, *J. Energy Chem.*, 2021, **56**, 365–373.

34 W. Sun, F. Wang, S. Hou, C. Yang, X. Fan, Z. Ma, T. Gao, F. Han, R. Hu, M. Zhu and C. Wang, *J. Am. Chem. Soc.*, 2017, **139**, 9775–9778.

35 C. Qiu, H. Huang, M. Yang, L. Xue, X. Zhu, Y. Zhao, M. Ni, T. Chen and H. Xia, *Energy Storage Mater.*, 2024, **72**, 103736.

36 X. Qian, T. Chen, Y. Wang, Q. Zhang, W. Li and J. Fu, *Angew. Chem., Int. Ed.*, 2025, **64**, e202412989.

37 S. Zhang, M. Ye, Y. Zhang, Y. Tang, X. Liu and C. C. Li, *Adv. Funct. Mater.*, 2023, **33**, 2208230.

38 I. R. Tay, J. Xue and W. S. V. Lee, *Adv. Sci.*, 2023, **10**, 2303211.

39 W. Jiang, K. Zhu and W. Yang, *Chem. – Eur. J.*, 2023, **29**, e202301769.

40 C. Xiudong, Z. Hang, L. Jin-Hang, G. Yun, C. Xiaohua, Z. Changchao, W. Yawei, W. Shitao, C. Shu-Lei, D. Shi-Xue and C. Dapeng, *Energy Storage Mater.*, 2022, **50**, 21–46.

41 W. Wang, C. Yang, X. Chi, J. Liu, B. Wen and Y. Liu, *Energy Storage Mater.*, 2022, **53**, 774–782.

42 D. Zhao, Q. Zhu, X. Li, M. Dun, Y. Wang and X. Huang, *Batteries Supercaps*, 2022, **5**, e202100341.

43 S. Chen, K. Li, K. S. Hui and J. Zhang, *Adv. Funct. Mater.*, 2020, **30**, 2003890.

44 F. Ming, H. Liang, Y. Lei, S. Kandambeth, M. Eddaoudi and H. N. Alshareef, *ACS Energy Lett.*, 2018, **3**, 2602–2609.

45 P. He, M. Yan, G. Zhang, R. Sun, L. Chen, Q. An and L. Mai, *Adv. Energy Mater.*, 2017, **7**, 1601920.

46 L. Wang, Z. Wu, M. Jiang, J. Lu, Q. Huang, Y. Zhang, L. Fu, M. Wu and Y. Wu, *J. Mater. Chem. A*, 2020, **8**, 9313–9321.

47 C. Chen, T. Wang, X. Zhao, A. Wu, S. Li, N. Zhang, X. Qu, L. Jiao and Y. Liu, *Adv. Funct. Mater.*, 2023, **34**, 2308508.

48 X. Li, X. Ma, Y. Hou, Z. Zhang, Y. Lu, Z. Huang, G. Liang, M. Li, Q. Yang, J. Ma, N. Li, B. Dong, Q. Huang, F. Chen, J. Fan and C. Zhi, *Joule*, 2021, **5**, 2993–3005.

49 Y. Fu, Q. Wei, G. Zhang, X. Wang, J. Zhang, Y. Hu, D. Wang, L. Zuin, T. Zhou, Y. Wu and S. Sun, *Adv. Energy Mater.*, 2018, **8**, 1801445.

50 N. Zhang, F. Cheng, J. Liu, L. Wang, X. Long, X. Liu, F. Li and J. Chen, *Nat. Commun.*, 2017, **8**, 405.

51 L. Junpeng, Y. Xubo, W. Jinwei, M. Chunjie, W. Tingxia, L. Nailiang, P. Xiufen, Z. Qian, W. Chao and L. Xifei, *Energy Storage Mater.*, 2025, **74**, 103887.

52 H. Wang, R. Guo, Y. Ma and F. Zhou, *Adv. Funct. Mater.*, 2023, **33**, 2301351.

53 K. Wang, J. Wang, P. Chen, M. Qin, C. Yang, W. Zhang, Z. Zhang, Y. Zhen, F. Fu and B. Xu, *Small*, 2023, **19**, 2300585.

54 D. Xie, Y. Wang, L. Tian, H. Huang, J. Sun, D.-W. Kim, J. Zhao and J. Mao, *Adv. Funct. Mater.*, 2025, **35**, 2413993.

55 W. Kao-ian, J. Sangsawang, M. Gopalakrishnan, S. Wannapaiboon, A. Watwiangkham, S. Jungsuttiwong, J. Theerthagiri, M. Y. Choi and S. Kheawhom, *ACS Appl. Mater. Interfaces*, 2024, **16**, 56926–56934.

56 Z. Wang, D. Zhou, Z. Zhou, W. Gong, S. Zhao, Y. Ling, F. Liu, J. Guo, K. Zhao, J. Wu, P. Xue, C. Li, Y. Sun, J. Luo, Z. Wang, J. Xu, L. Wei and Q. Zhang, *Adv. Funct. Mater.*, 2024, **34**, 2313371.

57 L. Zhang, L. Chen, X. Zhou and Z. Liu, *Adv. Energy Mater.*, 2015, **5**, 1400930.

58 G. Kasiri, R. Trócoli, A. Bani Hashemi and F. La Mantia, *Electrochim. Acta*, 2016, **222**, 74–83.

59 Z. Liu, P. Bertram and F. Endres, *J. Solid State Electrochem.*, 2017, **21**, 2021–2027.

60 K. Lu, B. Song, J. Zhang and H. Ma, *J. Power Sources*, 2016, **321**, 257–263.

61 R. Trócoli and F. La Mantia, *ChemSusChem*, 2015, **8**, 481–485.

62 L. Ma, S. Chen, C. Long, X. Li, Y. Zhao, Z. Liu, Z. Huang, B. Dong, J. A. Zapien and C. Zhi, *Adv. Energy Mater.*, 2019, **9**, 1902446.

63 Y. Zeng, X. F. Lu, S. L. Zhang, D. Luan, S. Li and X. W. D. Lou, *Angew. Chem., Int. Ed.*, 2021, **60**, 22189–22194.

64 W. Liubin, L. Ningbo, L. Qiaqia, W. Xiaohan, L. Jing, X. Yinuo, L. Zhiqiang, Z. Ning and L. Fujun, *Angew. Chem., Int. Ed.*, 2024, **64**, e20241639.

65 Q.-Q. Sun, T. Sun, J.-Y. Du, K. Li, H.-M. Xie, G. Huang and X.-B. Zhang, *Adv. Mater.*, 2023, **35**, 2301088.

66 F. Wan, L. Zhang, X. Wang, S. Bi, Z. Niu and J. Chen, *Adv. Funct. Mater.*, 2018, **28**, 1804975.

67 K. W. Nam, S. S. Park, R. Dos Reis, V. P. Dravid, H. Kim, C. A. Mirkin and J. F. Stoddart, *Nat. Commun.*, 2019, **10**, 4948.

68 Y. Zhao, S. Guo, M. Chen, B. Lu, X. Zhang, S. Liang and J. Zhou, *Nat. Commun.*, 2023, **14**, 7080.

69 Z. Ju, Q. Zhao, D. Chao, Y. Hou, H. Pan, W. Sun, Z. Yuan, H. Li, T. Ma, D. Su and B. Jia, *Adv. Energy Mater.*, 2022, **12**, 2201074.

70 X. Yu, Z. Li, X. Wu, H. Zhang, Q. Zhao, H. Liang, H. Wang, D. Chao, F. Wang, Y. Qiao, H. Zhou and S.-G. Sun, *Joule*, 2023, **7**, 1145–1175.

71 D. Chao, W. Zhou, F. Xie, C. Ye, H. Li, M. Jaroniec and S.-Z. Qiao, *Sci. Adv.*, 2020, **6**, 4098.

72 Q. Zhang, J. Luan, Y. Tang, X. Ji and H. Wang, *Angew. Chem., Int. Ed.*, 2020, **59**, 13180–13191.

73 Y. Zeng, D. Luan and X. W. Lou, *Chem*, 2023, **9**, 1118–1146.

74 H. Li, C. Guo, T. Zhang, P. Xue, R. Zhao, W. Zhou, W. Li, A. Elzatahry, D. Zhao and D. Chao, *Nano Lett.*, 2022, **22**, 4223–4231.

75 Q. Yang, G. Liang, Y. Guo, Z. Liu, B. Yan, D. Wang, Z. Huang, X. Li, J. Fan and C. Zhi, *Adv. Mater.*, 2019, **31**, 1903778.

76 J. Chen, W. Zhao, J. Jiang, X. Zhao, S. Zheng, Z. Pan and X. Yang, *Energy Storage Mater.*, 2023, **59**, 102767.

77 Q. Zhang, Y. Su, Z. Shi, X. Yang and J. Sun, *Small*, 2022, **18**, 2203583.

78 Z. Wang, M. Zhang, W. Ma, J. Zhu and W. Song, *Small*, 2021, **17**, 2100219.

79 L. Li, L. Wang, T. Ye, H. Peng and Y. Zhang, *Small*, 2021, **17**, 2005015.

80 M. Li, Q. He, Z. Li, Q. Li, Y. Zhang, J. Meng, X. Liu, S. Li, B. Wu, L. Chen, Z. Liu, W. Luo, C. Han and L. Mai, *Adv. Energy Mater.*, 2019, **9**, 1901469.

81 C. Wu, K. Xie, K. Ren, S. Yang and Q. Wang, *Dalton Trans.*, 2020, **49**, 17629.

82 Q. Lu, C. Liu, Y. Du, X. Wang, L. Ding, A. Omar and D. Mikhailova, *ACS Appl. Mater. Interfaces*, 2021, **13**, 16869.

83 B. Liu, M. Yang, W.-Y. Zhou, H.-W. Cai, S.-L. Zhong, M.-S. Zheng and Z.-M. Dang, *Energy Storage Mater.*, 2020, **27**, 205.

84 J. Zheng, Z. Huang, Y. Zeng, W. Liu, B. Wei, Z. Qi, Z. Wang, C. Xia and H. Liang, *Nano Lett.*, 2022, **22**, 1017.

85 S. Li, J. Fu, G. Miao, S. Wang, W. Zhao, Z. Wu, Y. Zhang and X. Yang, *Adv. Mater.*, 2021, **33**, 2008424.

86 C. Zhang, J. Chen, W. Xuan, S. Huang, B. You, W. Li, L. Sun, H. Jin, X. Wang, S. Dong, J. Luo, A. J. Flewitt and Z. L. Wang, *Nat. Commun.*, 2020, **11**, 1634.

87 H. Tian, Z. Li, G. Feng, Z. Yang, D. Fox, M. Wang, H. Zhou, L. Zhai, A. Kushima, Y. Du, Z. Feng, X. Shan and Y. Yang, *Nat. Commun.*, 2021, **12**, 237.

88 L. Hong, L.-Y. Wang, Y. Wang, X. Wu, W. Huang, Y. Zhou, K.-X. Wang and J.-S. Chen, *Adv. Sci.*, 2022, **9**, 2104866.

89 H. Liu, J.-G. Wang, W. Hua, L. Ren, H. Sun, Z. Hou, Y. Huyan, Y. Cao, C. Wei and F. Kang, *Energy Environ. Sci.*, 2022, **15**, 1872–1881.

90 Q. Wen, H. Fu, Y.-d. Huang, R.-d. Cui, H.-z. Chen, R.-h. Ji, L.-b. Tang, C. Yan, J. Mao, K.-h. Dai, Q. Wu, X.-h. Zhang and J.-c. Zheng, *Nano Energy*, 2023, **117**, 108810.

91 X. Liu, Q. Han, Q. Ma, Y. Wang and C. Liu, *Small*, 2022, **18**, 2203327.

92 P. Jiang, Q. Du, C. Lei, C. Xu, T. Liu, X. He and X. Liang, *Chem. Sci.*, 2024, **15**, 3357–3364.

93 V. Aupama, J. Sangsawang, W. Kao-ian, S. Wannapaiboon, J. Pimoei, W. Yoopensuk, M. Opchoei, Z. Tehrani, S. Margadonna and S. Kheawhom, *Electrochim. Acta*, 2024, **506**, 145059.

94 D. Li, J. Long, X. Liu, X. Chen, Z. Li and G. Lei, *Energy Fuels*, 2025, **39**, 8742–8752.

95 M. T. Hlaing, M. Gopalakrishnan, S. Praserthdam, W.-R. Liu, A. A. Mohamad, S. Rajendran, I. In and S. Kheawhom, *Chem. Eng. J.*, 2025, **509**, 161327.

96 H. Yang, K. Zhu, W. Xie and W. Yang, *ACS Nano*, 2025, **19**, 1433–1446.

97 J. Dong, J. Duan, R. Cao, W. Zhang, K. Fang, H. Yang, Y. Liu, Z. Shen, F. Li, R. Liu, M. Jin, L. Lei, H. Li and C. Chen, *SusMat*, 2024, **4**, e89.

98 C. Zhang, J. Holoubek, X. Wu, A. Daniyar, L. Zhu, C. Chen, D. P. Leonard, I. A. Rodríguez-Pérez, J.-X. Jiang, C. Fang and X. Ji, *Chem. Commun.*, 2018, **54**, 14097–14099.

99 F. Wang, O. Borodin, T. Gao, X. Fan, W. Sun, F. Han, A. Faraone, J. A. Dura, K. Xu and C. Wang, *Nat. Mater.*, 2018, **17**, 543–549.

100 H. Jiaqi, C. Xiaowei, W. Jing, L. Jianjun and L. Yu, *Chem. Eng. J.*, 2021, **430**, 133058.

101 H.-B. Chen, H. Meng, T.-R. Zhang, Q. Ran, J. Liu, H. Shi, G.-F. Han, T.-H. Wang, Z. Wen, X.-Y. Lang and Q. Jiang, *Angew. Chem., Int. Ed.*, 2024, **63**, e202402327.

102 Z. Jiao, X. Cai, X. Wang, Y. Li, Z. Bie and W. Song, *Adv. Energy Mater.*, 2023, **13**, 2302676.

103 Y. Liu, S. Liu, X. Xie, Z. Li, P. Wang, B. Lu, S. Liang, Y. Tang and J. Zhou, *InfoMat*, 2023, **5**, e12374.

104 Q. Chen, S. Chen, J. Ma, S. Ding and J. Zhang, *Adv. Funct. Mater.*, 2024, **34**, 2308272.

105 J. Liu, S. Chen, W. Shang, J. Ma and J. Zhang, *Adv. Funct. Mater.*, 2025, **35**, 2422081.

106 L. Kang, J. Zheng, K. Yue, H. Yuan, J. Luo, Y. Wang, Y. Liu, J. Nai and X. Tao, *Small*, 2023, **19**, 2304094.

107 W. Yan, Y. Liu, J. Qiu, F. Tan, J. Liang, X. Cai, C. Dai, J. Zhao and Z. Lin, *Nat. Commun.*, 2024, **15**, 9702.

108 A. VahidMohammadi, J. Rosen and Y. Gogotsi, *Science*, 2021, **372**, eabf1581.

109 M. Naguib, M. W. Barsoum and Y. Gogotsi, *Adv. Mater.*, 2021, **33**, 2103393.

110 B. Anasori and Y. Gogotsi, *Graphene 2D Mater. Technol.*, 2022, **7**, 75–79.

111 M. Naguib, O. Mashtalir, J. Carle, V. Presser, J. Lu, L. Hultman, Y. Gogotsi and M. W. Barsoum, *ACS Nano*, 2012, **6**, 1322–1331.

112 M. Ghidiu, M. R. Lukatskaya, M.-Q. Zhao, Y. Gogotsi and M. W. Barsoum, *Nature*, 2014, **516**, 78–81.

113 P. Urbankowski, B. Anasori, T. Makaryan, D. Er, S. Kota, P. L. Walsh, M. Zhao, V. B. Shenoy, M. W. Barsoum and Y. Gogotsi, *Nanoscale*, 2016, **8**, 11385–11391.

114 M. Li, J. Lu, K. Luo, Y. Li, K. Chang, K. Chen, J. Zhou, J. Rosen, L. Hultman, P. Eklund, P. O. Å. Persson, S. Du, Z. Chai, Z. Huang and Q. Huang, *J. Am. Chem. Soc.*, 2019, **141**, 4730–4737.

115 W. Sun, S. A. Shah, Y. Chen, Z. Tan, H. Gao, T. Habib, M. Radovic and M. J. Green, *J. Mater. Chem. A*, 2017, **5**, 21663–21668.

116 Y. Cao, C. Guo and Y. Zou, *Mater. Sci. Technol.*, 2019, **35**, 1904–1907.

117 D. Geng, X. Zhao, Z. Chen, W. Sun, W. Fu, J. Chen, W. Liu, W. Zhou and K. P. Loh, *Adv. Mater.*, 2017, **29**, 1702678.

118 R. Chen, K. Rui, X. Yang, A. Huang, Y. Zhang, H. Lin, Y. Yan, J. Zhu and W. Huang, *Chem. Commun.*, 2018, **55**, 771–774.

119 P. A. Maughan, N. Tapia-Ruiz and N. Bimbo, *Electrochim. Acta*, 2020, **341**, 136061.

120 X. Li, M. Li, Q. Yang, D. Wang, L. Ma, G. Liang, Z. Huang, B. Dong, Q. Huang and C. Zhi, *Adv. Energy Mater.*, 2020, **10**, 2001394.

121 N. Zhang, S. Huang, Z. Yuan, J. Zhu, Z. Zhao and Z. Niu, *Angew. Chem., Int. Ed.*, 2021, **60**, 2861–2865.

122 Y. Tian, Y. An, Y. Yang and B. Xu, *Energy Storage Mater.*, 2022, **49**, 122–134.

123 X. Li, M. Li, K. Luo, Y. Hou, P. Li, Q. Yang, Z. Huang, G. Liang, Z. Chen, S. Du, Q. Huang and C. Zhi, *ACS Nano*, 2022, **16**, 813–822.

124 C. Sun, C. Wu, X. Gu, C. Wang and Q. Wang, *Nano–Micro Lett.*, 2021, **13**, 89.

125 Q. Wang, M. Wang, L. Wen, W. Zeng, B. Ge, C. Zhang, Y. Yue and S. Wang, *Adv. Funct. Mater.*, 2023, **34**, 2214506.